

**Temporal Monitoring of *Zostera marina* Along the Eastern Coast of  
James Bay Utilizing Multispectral Landsat Imagery and Random  
Forests Classifier**

by

Kevin R. Clyne

B.Sc. Marine Science, University of Maine, 2018

A Thesis Submitted in Partial Fulfillment  
of the Requirements for the Degree of

**Master of Science in Environmental Management**

in the Graduate Academic Unit of Forestry and Environmental Management

Supervisor: Brigitte Leblon, Ph.D., Forestry and Environmental  
Management  
Myriam Barbeau, Ph.D., Biology  
Maycira Costa, Ph.D., Geography

Examining Board: Ian Church, Ph.D., Geodesy and Geomatics Engineering  
Feng Rui-Ming, Ph.D., Forestry and Environmental  
Management

This thesis is accepted by the  
Dean of Graduate Studies

THE UNIVERSITY OF NEW BRUNSWICK

October 2022

© Kevin Clyne, 2022

## ABSTRACT

Along the eastern coastline of James Bay, also known to the local Cree as Eeyou-Istchee, exist large subtidal eelgrass meadows. This study assessed the feasibility of evaluating the distribution of eelgrass beds along the entire eastern coastline of James Bay using imagery from the Landsat-8 Operational Land Imager and supervised classification using random forests machine learning algorithm. The methodology was then applied to historical imagery from the Landsat archive (Landsat-5 Multispectral Instrument), and image classifications were evaluated for accuracy using a randomly generated subset of digitized eelgrass distribution maps from Hydro-Quebec. Our classified images from 1988, 1991, 1996, and 2019 achieved overall accuracies ranging from 74.6 – 84.6% when evaluated using our ground-truth datasets. Our supervised classification approach showed the ability to detect eelgrass along the entire coast where turbid water was not present. The total area classified as eelgrass appeared to decrease over the study period (1988 – 2019).

## ACKNOWLEDGEMENTS

I would like to thank my advisory committee: Dr. Brigitte Leblon, Dr. Armand LaRocque, Dr. Maycira Costa, Dr. Myriam Barbeau, and Dr. Mélanie-Louise Leblanc for their guidance, assistance, and willingness to help. I would also like to thank MITACS and the Niskamoon Corporation for their financial support, the members of the CHCRP Eelgrass team (Dr. Mary O'Connor, Kaleigh Davies, Dr. Fanny Noisette, Dr. Mélanie-Louise Leblanc) who collected field data during the summer of 2019, as well as Ernie Rabbitskin, Geraldine Mark, Marc Dunn, and the Cree people who generously lent their knowledge, land, and resources to help make this research possible.

## TABLE OF CONTENTS

ABSTRACT .....	ii
ACKNOWLEDGEMENTS.....	iii
TABLE OF CONTENTS .....	iv
LIST OF TABLES.....	vi
LIST OF FIGURES.....	vii
CHAPTER 1: GENERAL INTRODUCTION.....	1
REFERENCES.....	4
CHAPTER 2: USE OF LANDSAT-8 OLI IMAGERY AND LOCAL INDIGENOUS KNOWLEDGE FOR EELGRASS MAPPING IN EYYOU ISTCHEE .....	6
2.1. ABSTRACT .....	6
2.2. INTRODUCTION .....	7
2.3. MATERIALS AND METHODS .....	10
2.3.1. Study Area .....	10
2.3.2. Image Acquisition.....	11
2.3.3. Field Data .....	12
2.3.4. Image Processing.....	13
2.3.5. Training Areas.....	15
2.3.6. Additional Input Layers.....	16
2.3.7. Random Forests Classifier .....	17
2.4. RESULTS .....	18
2.4.1. Class Separability.....	18
2.4.2. Classification.....	22
2.5. DISCUSSION AND CONCLUSIONS.....	28
2.6. REFERENCES.....	31

CHAPTER 3: USE OF LANDSAT IMAGERY TIME SERIES AND RANDOM FORESTS CLASSIFIER TO RECONSTRUCT EELGRASS BED DISTRIBUTION MAPS IN EEYOU ISTCHEE.....	36
3.1. ABSTRACT .....	36
3.2. INTRODUCTION .....	37
3.3. MATERIALS AND METHODS .....	42
3.3.1. Study Area .....	42
3.3.2. Image Selection and Acquisition .....	43
3.3.3. Other Data.....	45
3.3.4. Image Processing.....	48
3.3.5. Model Training Data .....	52
3.3.6. Image Classification.....	54
3.3.7. Accuracy Assessment.....	55
3.3.8. Comparison To Aerial Photos.....	56
3.4. RESULTS .....	58
3.4.1. Image Classification and Validation .....	58
3.4.2. Comparison to Historical Aerial Photos.....	71
3.5. DISCUSSION .....	80
3.5.1. Overall Mapping Accuracy .....	80
3.5.3. Variable Importance in Random Forests.....	81
3.5.4. Comparison to HQ Aerial Photographs.....	82
3.5.2. Eelgrass Distribution and Temporal Trends.....	70
3.5.5. Study Limitations.....	87
3.6. CONCLUSIONS.....	90
3.7. REFERENCES.....	92
CHAPTER 4: GENERAL DISCUSSION .....	100
REFERENCES.....	106
Appendix.....	109
Curriculum Vitae	

## LIST OF TABLES

<b>Table</b>		<b>Page</b>
2.1	List of the Landsat-8 OLI images used in the study and associated dates, times, and tide heights	12
2.2	Number of ground-truth data points coming from each dataset for each ground-truth point class	13
2.3	Spectral variables added to the classifier derived from the original band reflectance	17
2.4	J-M distances computed with the class training areas for the Landsat-8 OLI bands of the September image mosaic.	21
2.5	Confusion matrix for out-of-bag training pixels computed with the Random Forests classifier.	22
2.6	Validation accuracies obtained by comparing field-based ground-truth sites with the classified image.	28
3.1	List of the images used in the study and associated date and cloud cover	45
3.2	Wavelengths of the Landsat-5 and Landsat-8 bands of the images used in the study	50
3.3	Vegetation indices and bathymetric ratios considered in our study.	51
3.4	Number of training pixels used to train the Random Forests model according to the year and class	52
3.5	Spectral separability between classes using J-M distances computed with the combination of original spectral bands, the vegetation indices, and the bathymetric ratios for each Landsat sensor.	59
3.6	Confusion matrices showing classification accuracy evaluated with the OOB training areas for each classification year, expressed as a percentage of the total number of OOB training points for each year.	60-61
3.7	Importance of each input variable for increasing model accuracy ranked from the most (1) to the least important (24) as a function of the classification year	65
3.8	Confusion matrices showing classification accuracy evaluated with the ground-truth dataset for each classification year, expressed as a percentage of the total points used for each year.	67
3.9	Total classified eelgrass area, assessed with turbid water points from any classified image omitted from all other images, as well as with turbid water points included.	69

## LIST OF FIGURES

<b>Figure</b>		<b>Page</b>
2.1	Location of the four main Cree coastal communities along the Western coastline of Eeyou-Istchee	10
2.2	RGB composite for the mosaic created using Acolite with the images acquired over James Bay on September 16, 2019	14
2.3	Mean reflectance values for each class for the first 6 Landsat-8 bands for both images	19
2.4	Mean values of the Acolite variables computed during the atmospheric correction for each class for both images	19
2.5	Mean values of the vegetation indices used in the study for each class for both images	20
2.6	Mean values of each bathymetric ratio for each class for both images	20
2.7	Classified image produced by applying the Random Forests classifier to both Landsat-8 OLI images	23
2.8	Classified image produced by applying the Random Forests classifier to both Landsat-8 OLI images for the coastline around Chisasibi	24
2.9	Classified image produced by applying the Random Forests classifier to both Landsat-8 OLI images outlining the coastline around Wemindji	25
2.10	Classified image produced by applying the Random Forests classifier to both Landsat-8 OLI images outlining the coastline around Eastmain	26
2.11	Classified image produced by applying the Random Forests classifier to both Landsat-8 OLI images outlining the coastline around Waskaganish	27
3.1	Study area showing the two zones where eelgrass distribution was evaluated: North and South of the Cree community of Chisasibi	43
3.2.	Digitized historical eelgrass bed distribution maps overlaid over a Google Earth image as a function of the year. Data outside of the red box was excluded from the study area due to varying survey extents	47
3.3	Locations of sites where aerial photographs with delineations of eelgrass extent were published	57
3.4	Classified images produced by applying the Random Forests classifier to all the reflectance images, associated vegetation indices, and bathymetric ratios for each year	62-63
3.5	Evolution of the eelgrass area extracted from the classified imagery as a function of the classification year. The dotted lines represent trends over the course of the study period, since no data exists between 1996 and 2019.	68

3.6	Comparison between the classified Landsat imagery of 1988 and the aerial photographs of 1986 for the limits of eelgrass distribution at sites 7-13.	72-74
3.7	Comparison between the classified Landsat imagery of 1996 and the aerial photographs of 1995 for the limits of eelgrass distribution at sites 3-13.	75-78
3.8	Evolution of the yearly burned areas extracted from the fire map of the Quebec Ministry of Forests, Wildlife and Parks website ( <a href="https://mffp.gouv.qc.ca/">https://mffp.gouv.qc.ca/</a> )	83
3.9	Distribution of the 1989 wildfires in Eeyou Istchee. Source: Quebec Ministry of Forests, Wildlife and Parks website ( <a href="https://mffp.gouv.qc.ca/">https://mffp.gouv.qc.ca/</a> )	84
3.10	Comparison between Landsat RGB composites over major tributaries of the eastern coast of James Bay before and after the 1989 wildfires	85-86

## CHAPTER 1: GENERAL INTRODUCTION

Seagrass exists worldwide in littoral, intertidal, and subtidal ecosystems and is a vital component of many healthy coastal habitats[1–3]. James Bay (the southernmost extension of Hudson Bay and consequently the Arctic Ocean) has historically been known to contain large meadows of eelgrass (*Zostera marina*), a true seagrass native to the Northern Hemisphere, within its shallow depths [2,4]. The region has historically been primarily utilized by the indigenous Cree people, who today have four main settlements along the coast of the Bay (from North to South: Chisasibi, Wemindji, Eastmain, and Waskaganish) [5]. Eelgrass has a prominent place in the culture of the Cree, who utilize the coastline for subsistence hunting [6]. Eelgrass is known to provide shelter for juvenile fish and invertebrates and food for migratory waterfowl, both of which are essential components of the Cree diet [7,8]. Eelgrass in James Bay may also be of global importance, as seagrasses worldwide are known to sequester carbon [9,10].

Today, the eastern coastline of James Bay is heavily utilized by the power supply company Hydro-Quebec, who in the 1970s undertook a massive hydroelectric development known as the James Bay Project that severely altered the hydrology of the area as well as many of the ecosystems on and surrounding the coast [11,12]. This prompted investigations by Hydro-Quebec into the distribution of eelgrass along the coast and the impacts and ramifications of their

hydroelectric project. Eelgrass along the coast was generally assessed by Hydro-Quebec using aerial photography taken by helicopter survey and/or intense monitoring of individual bed sites [13,14]. Besides a large-scale and universal decline in eelgrass bed health and distribution in 1999 (for which the cause is unclear), they determined that the hydroelectric development had little impact on eelgrass growth in the bay outside of the plume of the La Grande River (the site of the largest hydroelectric power generating station), and consistent monitoring became limited to field surveys assessing bed health at several individual sites every few years [15].

The eastern coastline of James Bay is relatively shallow (the average depth across the entire bay is 28m), a result of large amounts of riverine input and, primarily, isostatic rebound [16]. This presents multiple obstacles for researchers hoping to map and quantify eelgrass and other coastal features; the shoreline is difficult to navigate and dotted by bays and islands, and large boats cannot travel along much of the coast due to water depth. The bay is frozen for large parts of the year (October – June), and weather can be highly variable, making field surveys challenging in their scope and ambition. Most major studies investigating eelgrass distribution in the bay have been carried out via Hydro-Quebec, by capturing aerial photos using a helicopter. These data were collected in different years and then ceased before the turn of the century, leaving us in the

present with distribution maps for various years in the late 1980s-1990s, a few aerial photographs, and little more information about the current and projected status of health of eelgrass in James Bay.

An alternative approach to evaluating the current and historical distribution of eelgrass along James Bay's eastern coast is through the remote sensing of eelgrass using multispectral satellite imagery. Satellite remote sensing offers the possibility to provide a systematic approach to mapping and assessing eelgrass bed distribution along the eastern coast of James Bay that can integrate both past and present data. The Landsat data collection has data spanning from 1984 to the present day with high levels of comparability between images [17].

This thesis follows a paper-based format comprising two individual papers presented as Chapters 2 and 3, respectively. The first paper (Chapter 2) presents an assessment of the ability of Landsat-8 OLI imagery to detect and therefore map eelgrass bed distribution in 2019 along the eastern coastline of James Bay. The second paper (Chapter 3) utilizes historical imagery from the Landsat archive and historical data provided by Hydro-Quebec to evaluate temporal trends in eelgrass distribution along the eastern coastline of James Bay and provide a framework for satellite-based mapping objectives in the future. This study is part of a Cree-driven project, the Coastal Habitat Comprehensive

Research Program (CHCRP). The CHCRP aims to combine Cree's traditional knowledge with Western science to understand better environmental changes in the coastal ecosystems and ecosystem services of eastern James Bay.

## REFERENCES

1. Olesen, B.; Krause-Jensen, D.; Marbà, N.; Christensen, P. Eelgrass *Zostera marina* in Subarctic Greenland: Dense Meadows with Slow Biomass Turnover in Cold Waters. *Marine Ecology Progress Series* **2015**, *518*, 107–121, doi:10.3354/meps11087.
2. Lalumière, R.; Messier, D.; Fournier, J.J.; Peter McRoy, C. Eelgrass Meadows in a Low Arctic Environment, the Northeast Coast of James Bay, Québec. *Aquatic Botany* **1994**, *47*, 303–315, doi:10.1016/0304-3770(94)90060-4.
3. Poursanidis, D.; Topouzelis, K.; Chrysoulakis, N. Mapping Coastal Marine Habitats and Delineating the Deep Limits of the Neptune's Seagrass Meadows Using Very High-Resolution Earth Observation Data. *International Journal of Remote Sensing* **2018**, *39*, 8670–8687, doi:10.1080/01431161.2018.1490974.
4. Dignard, N.; Lalumière, R.; Reed, A.; Julien, M. *Habitats of the Northeast Coast of James Bay*; Environment Canada, Canada Wildlife Service, Occasional Paper Number 70, **1991**. 27p.
5. Royer, M.-J.S. Eastern James Bay and the Cree. In *Climate, Environment and Cree Observations: James Bay Territory, Canada*; Royer, M.-J.S., Ed.; SpringerBriefs in Climate Studies; Springer International Publishing: Cham, **2016**; pp. 35–61 ISBN 978-3-319-25181-3.
6. Prevett, J.P.; Lumsden, H.G.; Johnson, F.C. Waterfowl Kill by Cree Hunters of the Hudson Bay Lowland, Ontario. *ARCTIC* **1983**, *36*, 185–192, doi:10.14430/arctic2261.
7. Kollars, N.M.; Henry, A.K.; Whalen, M.A.; Boyer, K.E.; Cusson, M.; Eklöf, J.S.; Hereu, C.M.; Jorgensen, P.; Kiriakopolos, S.L.; Reynolds, P.L.; et al. Meta-Analysis of Reciprocal Linkages between Temperate Seagrasses and Waterfowl with Implications for Conservation. *Frontiers in Plant Science* **2017**, *8*, 2119, doi:10.3389/fpls.2017.02119.

8. Short, F.T.; Coles, R.G. Global Seagrass Research Methods. *Elsevier Science B.V., Amsterdam*. **2001**, 31–58.
9. Postlethwaite, V.R.; McGowan, A.E.; Kohfeld, K.E.; Robinson, C.L.K.; Pellatt, M.G. Low Blue Carbon Storage in Eelgrass (*Zostera marina*) Meadows on the Pacific Coast of Canada. *PLOS ONE*. **2018**. *13*, e0198348, doi: 10.1371/journal.pone.0198348.
10. Potouroglou, M.; Bull, J.C.; Krauss, K.W.; Kennedy, H.A.; Fusi, M.; Daffonchio, D.; Mangora, M.M.; Githaiga, M.N.; Diele, K.; Huxham, M. Measuring the Role of Seagrasses in Regulating Sediment Surface Elevation. *Scientific Reports* **2017**, *7*, 1–11, doi:10.1038/s41598-017-12354-y.
11. Marsh, J.H. James Bay Project. *The Canadian Encyclopedia*. **2015**. <https://www.thecanadianencyclopedia.ca/en/article/james-bay-project>
12. Milko, R. Potential Ecological Effects of the Proposed GRAND Canal Diversion Project on Hudson and James Bays. *ARCTIC* **1986**, *39*, 316–326. doi:10.14430/arctic2094.
13. Lalumière, R. *Étude de La Zostère Marine (Zostera marina) Sur La Côte Est de La Baie James - Été 1986*; **1986**. 112p.
14. Hydro-Quebec and GENIVAR Groupe Conseil Inc. *Environmental Monitoring of the La Grande Complex. Abridged Summary Report 1988-2000. Eelgrass Meadows of the Northeast Coast of James Bay.*; **2005**. 42p.
15. Hayeur, G. Summary of Knowledge Acquired in Northern Environments from 1970 to 2000. *Montreal: Hydro-Quebec* **2001**. 113p.
16. El-Sabh, M.I.; Koutitonsky, V.G. An Oceanographic Study of James Bay before the Completion of the La Grande Hydroelectric Complex. *ARCTIC* **1977**, *30*, 169–186, doi:10.14430/arctic2697.
17. Historic Landsat 5 Mission Ends | Landsat Science Available online: <https://landsat.gsfc.nasa.gov/article/historic-landsat-5-mission-ends/> (accessed on 24 June 2022).

**CHAPTER 2: USE OF LANDSAT-8 OLI IMAGERY AND LOCAL  
INDIGENOUS KNOWLEDGE FOR EELGRASS MAPPING IN EEYOU**

**ISTCHEE<sup>1</sup>**

**2.1. ABSTRACT**

The eastern coastline of James Bay (Eeyou Istchee) is known to be home to beds of subarctic eelgrass (*Zostera marina* L.). These eelgrass beds provide valuable habitat and food sources for coastal and marine animals and contribute to valuable ecosystem services such as stabilizing the shoreline all along the coast. Despite reports from Cree communities that eelgrass bed health has declined, limited research has been performed to assess and map the spatial distribution of eelgrass within the bay. This study aims to address that issue by evaluating the capability of Landsat-8 Operational Land Imager (OLI) imagery to establish a baseline map of eelgrass distribution in 2019 in the relatively turbid waters of Eeyou Istchee. Three images acquired in September 2019 were merged and classified using Random Forests into the following classes: Eelgrass, Turbid Water, Highly Turbid Water, and Optically Deep Water. The resulting classified

---

<sup>1</sup> This chapter was published in Clyne, K., Leblon, B., LaRocque, A., Costa, M., Leblanc, M., Rabbitskin, E., & Dunn, M. (2021). Use of Landsat-8 Oli Imagery and Local Indigenous Knowledge for Eelgrass Mapping in Eeyou Istchee. *ISPRS Annals of the Photogrammetry, Remote Sensing and Spatial Information Sciences*, V-3–2021, 15–22. <https://doi.org/10.5194/isprs-annals-v-3-2021-15-2021>

image was validated against 108 ground truth data obtained from both the eelgrass health and Hydro-Quebec research teams. The resulting overall accuracy was 78.7%, indicating the potential of the Random Forests classifier to estimate baseline eelgrass coverage in James Bay using Landsat-8 imagery. This project is part of a Cree-driven project, the Coastal Habitat Comprehensive Research Program (CHCRP). The CHCRP aims to combine Cree's traditional knowledge with Western science to understand better environmental changes in the coastal ecosystems and ecosystem services of eastern James Bay. The study is funded by a MITACS grant sponsored by Niskamoon Corporation, an indigenous non-profit organization.

## 2.2. INTRODUCTION

*Zostera marina* L., more commonly known as eelgrass, is a marine flowering plant found in many coastal marine environments across the Northern Hemisphere [18]. It occurs primarily in the sublittoral zone, in areas sheltered from wave action with a soft or sandy substrate, and is generally submerged at low tide. Seagrasses, including eelgrass, provide a wide variety of ecosystem services, which make them an important indicator of environmental health [19,20]. Some of the services they provide include protection from wave and tidal action, shelter for juvenile fish and invertebrates [21,22], carbon sequestration [23], and a foraging environment for migratory and/or residential waterfowl

[7,24]. Seagrasses can also play an important role in sediment stabilization and erosion reduction [10], making them an essential feature for coastline preservation [25]. The Eastern coastline of James Bay, Quebec (also referred to as Eeyou Istchee by the Cree First Nation) offers an excellent growing environment for eelgrass [2]. The coastline is dotted with numerous islands providing shelter from wind and wave action [26], and coastal development by humans is low. In Eeyou Istchee, eelgrass beds are critical food for waterfowl [27], particularly for the Canada Geese (*Branta canadensis*) and Atlantic Brant (*B. bernicla rota*), as documented by the Cree hunter experience and described in Dignard et al. (1991) [4], COMEX (2013) [28] and Royer (2016) [5]. To this day, migratory waterfowl hunting is an important activity in coastal communities and contributes to maintaining traditional food security.

Eeyou Istchee has been subject to climate change and large-scale hydroelectric development in the past fifty years. Hydroelectric development in the eastern James Bay watershed, which began in the 1970s, has entailed diverting water from the Ungava Bay watershed and the Rupert and Eastmain Rivers of southern James Bay into the La Grande River watershed that drains into northeast James Bay. Although the coastal zones have been monitored since the early 1980s, many hydrological changes and implications for eelgrass distribution within the bay are largely understudied. The Cree Land Users of

Eeyou-Istchee have noted steady declines in eelgrass coverage along the coast, primarily near Chisasibi, in the late 1980s, and then a drastic decline in 1997-1998 [29]. Cree report that since the decline in the late 1990s, eelgrass recovery has been very slow, and the eelgrass currently observed in some areas seems unhealthy (e.g., shorter, less dense, discolored) [29]. Due to the inaccessibility of much of the coastline, quantifying and mapping eelgrass extent within the bay presents a major challenge. Multispectral satellite imagery offers the only source of continuous data spanning the entire extent of the coastline, and much of it is freely available. The objectives of this study are to assess the capability of the Landsat-8 Operational Land Imager (OLI) imagery to detect eelgrass in Eeyou Istchee waters and map the distribution of eelgrass along the eastern coastline of James Bay in the summer of 2019. Temperate and subarctic water, such as in Eeyou Istchee, poses additional challenges for mapping eelgrass compared to tropical and subtropical waters because this region tends to have lower water clarity and, therefore, low light penetration, like West coast waters [30,31]. Local indigenous knowledge about the eelgrass beds was employed during field data collection. The study is part of a Cree-driven project, the Coastal Habitat Comprehensive Research Program (CHCRP), which aims to combine Cree's traditional knowledge with Western science to understand better environmental changes in the coastal ecosystems and ecosystem services of eastern James Bay.

## 2.3. MATERIALS AND METHODS

### 2.3.1. Study Area

The study area encompasses the entire Eastern coastline of James Bay, from about 54.7 °N latitude in the north to 51.1 °N in the south (Figure 2.1). James Bay represents the southernmost portion of Hudson Bay. Eastern James Bay is ice-covered between December and early June each year [16], although the date of fast ice breakup has gotten progressively earlier since 1980 [32].

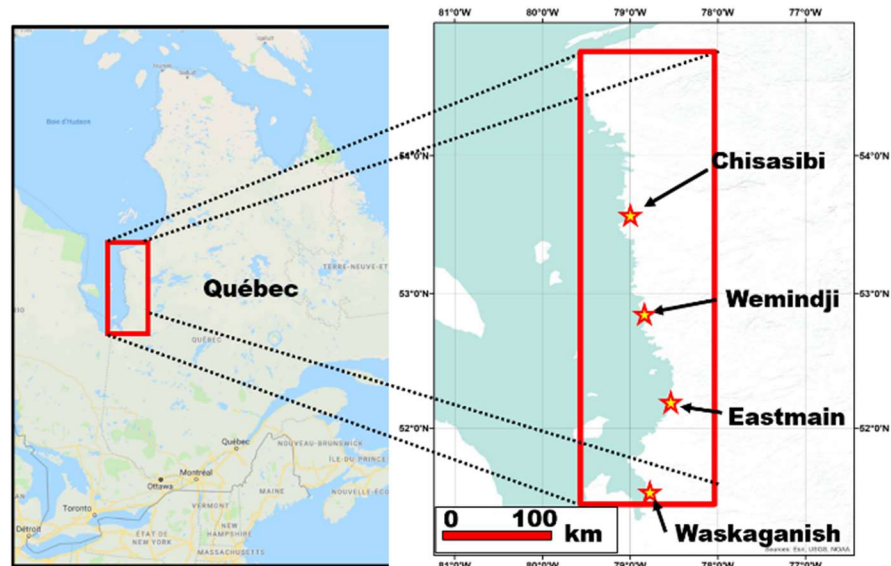


**Figure 2.1.** Location of the four main Cree coastal communities along the Western coast of Eeyou-Istchee.

James Bay is essentially a postglacial depression and, as such, is affected by the isostatic rebound. Thus, the eastern coastline can be characterized by having a low coastal slope and many islands that dot the shoreline, protecting it

from wind and tidal action. According to Dignard et al. (1991) [4], eelgrass meadows are abundant in every inlet along the eastern coast of James Bay, except at the mouth of large rivers. Towards the open sea, eelgrass meadows generally are replaced by a zone colonized by the brown algae *Fucus distichus* and *Ascophyllum nodosum* [4]. Four coastal communities, namely Chisasibi, Wemindji, Eastmain, and Waskaganish, with populations (primarily Cree First Nations) ranging from about 900 people in Eastmain to nearly 5000 people in Chisasibi, are located along this coast. Except for the hydroelectric development initiated in the early 1970s [11], there is little coastal development in the region.

### **2.3.2. Image Acquisition**

The study used freely available imagery acquired by the Landsat-8 OLI (Table 2.1). Images were obtained on the United States Geological Survey's (USGS) Earth Explorer website. Three images were acquired on September 16, 2019, during the period when the eelgrass reached its peak biomass [2]. Given that there was cloud cover over Chisasibi on the September image, we used a cloud-free image acquired on August 26, 2019, as close as possible to the September image.

**Table 2.1.** List of the Landsat-8 OLI images used in the study and associated dates, times, and tide heights.

Scene Identifier	Image Date	Image Time (UTC)	Tide Height (m)*
LC80200222019259LGN00	2019-09-16	16:12:59	1.1
LC80200232019259LGN00	2019-09-16	16:13:23	1.1
LC80200242019259LGN00	2019-09-16	16:13:47	1.1
LC80210222019234LGN00	2019-08-22	16:19:19	1.4

\*Tide height is predictive tide height acquired at <https://tides.gc.ca>

### 2.3.3. Field Data

Field data were acquired during the summer of 2019 from two different sources: Hydro-Quebec’s eelgrass monitoring program and the CHCRP’s field surveys [33] (Table 2.2). Both datasets evaluated eelgrass presence/absence at several sites throughout the study area that was determined using snorkeling surveys by SCUBA and snorkeling divers of the CHCRP eelgrass health team and Hydro-Québec. The location of the sites assessed by the CHCRP dataset was guided by local Cree land users who have a good understanding of their coastal environment. Each dataset recorded each point’s location using a GPS. The CHCRP dataset from the field research team was scored into two classes: eelgrass present and eelgrass absent. The Hydro-Quebec dataset scored eelgrass density at each site on a scale from 1-4, with 4 representing continuous eelgrass

and 1 representing a complete absence of eelgrass. To compare the two datasets, any score from 2-4 in the Hydro-Quebec dataset was considered eelgrass present. These field data were used to validate the final classified image mosaic. Points classified as turbid water were omitted from the validation analysis since the reflectance signal in turbid waters is dominated by particulate matter in the water column and, therefore, should not show the spectral signature of eelgrass.

**Table 2.2.** Number of ground-truth data points coming from each dataset for each ground-truth point class.

Dataset	Eelgrass Present	Eelgrass Absent	Turbid water in the classified image	Total
Hydro-Quebec	51	0	12	63
CHCRP Field Team	31	35	18	84
Total	82	35	36	147

#### 2.3.4. Image Processing

The four images obtained from the USGS EarthExplorer were top-of-atmosphere (TOA) reflectance images that were converted into surface reflectance images using Acolite, a free atmospheric correction software by the Royal Belgian Institute of Natural Sciences designed for simple and fast processing of coastal scenes [34]. The atmospheric correction in the Acolite software is based on the dark-spectrum fitting algorithm, and a sun glint correction is also applied during the correction [35]. Acolite was also used to

mosaic the three images acquired on September 16, 2019. Once processing was completed, the resulting image mosaic was clipped to the coastline. The September image mosaic produced by Acolite can be seen in Figure 2.2.

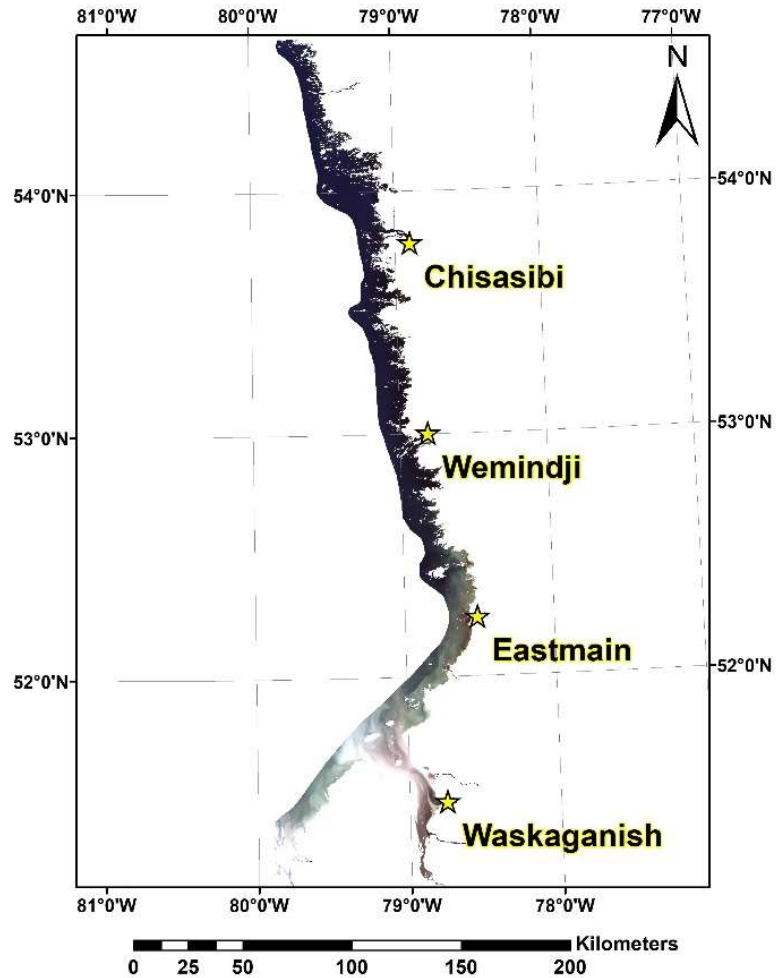


**Figure 2.2.** RGB composite for the mosaic created using Acolite with the images acquired over James Bay on September 16, 2019

### 2.3.5. Training Areas

The September mosaics and the August imagery were classified using the Random Forests supervised classifier, which requires training areas. Representative training areas were delineated through photointerpretation of the satellite imagery for the four following classes: Eelgrass (EG), Turbid Water (TW), Highly Turbid Water (HTW), and Optically Deep Water (DW). Spectral separability between representative training classes was assessed using Jeffries-Matusita (J-M) distance computed using Geomatica [36]. In the late summer of 2019, much of the eastern coastline of James Bay contained turbid water, either within bays near the coastline or out in deeper waters at the southern end of the bay (as exhibited in Figure 2.2). To account for this turbidity, a “Turbid Water” class was created through a manual selection of visibly turbid waters. Another class was created as “Highly turbid water”, which encompasses the reflectance signal of optically shallow sandy James Bay waters and visually highly turbid waters (water that appeared very light brown or red on RGB imagery). Optically shallow sandy waters showed a similar spectral curve to highly turbid waters, and both highly turbid waters and optically shallow waters displayed higher reflectance values than any other class in every visible band and the near-infrared band. To avoid conflating the two classes, these classes were merged.

Besides, the deep-water class was meant to encompass all optically deep water that should not contain eelgrass theoretically.

### **2.3.6. Additional Input Layers**

To bolster the potential separability between the four training classes, additional layers were created as inputs for the classifier. Concentration [37], Floating Algal Index [38], and orange reflectance [39]. The four layers are computed during the atmospheric correction. Additionally, we used 11 vegetation indices, as shown in Table 2.3. Finally, to separate optically deep-water areas, four bathymetric ratios were computed (Table 2.3). They are based on the ratio decay algorithm designed for evaluating satellite-derived bathymetry [40]. The computed layers were combined with the surface reflectance mosaic from Acolite and used as inputs for the RF classifier. Acolite provides the option to compute the so-called “L2W Parameters”, which include Turbidity [38], Suspended Material Concentration [37], Floating Algal Index [38], and orange reflectance [39]. The four layers are computed during the atmospheric correction. Additionally, we used 11 vegetation indices, as shown in Table 2.3. Finally, to separate optically deep-water areas, four bathymetric ratios were computed (Table 2.3). They are based on the ratio decay algorithm designed for evaluating satellite-derived bathymetry [40]. The computed layers

were combined with the surface reflectance mosaic from Acolite and used as inputs for the RF classifier.

**Table 2.3.** Spectral variables added to the classifier derived from the original band reflectance

Variable	Expression*
DVI	$NIR - R$
GDVI	$NIR - G$
GNDVI	$(NIR - G) / (NIR + G)$
NDVI	$(NIR - R) / (NIR + R)$
NG	$G / (NIR + R + G)$
NR	$R / (NIR + R + G)$
NNIR	$NIR / (NIR + R + G)$
RVI	$NIR / R$
GRVI	$NIR / G$
NDAVI	$(NIR - B) / (NIR + B)$
WAVI	$1.5 * (NIR - B) / (NIR + B + 0.5)$
Bathy 1	$\ln(B/G)$
Bathy 2	$\ln(Ub/G)$
Bathy 3	$\ln(B/R)$
Bathy 4	$\ln(Ub/R)$

\* NIR = NIR-Band (0.845 – 0.885  $\mu\text{m}$ ) reflectance, R = Red Band (0.630 – 0.680  $\mu\text{m}$ ) reflectance, G = Green Band (0.525 – 0.600  $\mu\text{m}$ ) reflectance, B = Blue Band (0.450 – 0.515  $\mu\text{m}$ ) reflectance, Ub = Ultrablue Band (0.433 – 0.453  $\mu\text{m}$ ) reflectance.

### 2.3.7. Random Forests Classifier

The classifier used is Random forests, a non-parametric, decision-tree classifier that does not assume a normal distribution of the input data [41]. Random forests can be run in two ways: “all-polygon” and “sub-polygon”. The all-polygon setting uses all the pixels within the training area polygons, while the sub-polygon version randomly selects a user-determined number of pixels from each training area polygon. For this study, the all-polygon setting was used, as it

has the advantage of considering the actual class size. The forest size was 500 independent decision trees. The *mtry* variable, which refers to the number of variables randomly sampled as candidates at each split of every node, was set to the default value (the square root of the total number of predictor variables, rounded down). The classifier randomly selects two-thirds of the training data (referred to as “In Bag” data) to develop one decision tree. This tree is then validated using the remaining third of the training data (referred to as “out of bag”, or OOB data). The process is repeated for the 500 individual decision trees and produces 500 independent classifications. These independent classifications are then combined to create the final classification. RF is not sensitive to noise or over-fitting and can estimate the importance of the individual input variables. The August image was classified separately from the September mosaic, and the area covered by clouds was clipped from the August classified image and mosaicked together on the September image to create one classified image mosaic. The classification accuracy assessment and the ground-truth validation accuracy assessment use the combined data from both image classifications.

## 2.4. RESULTS

### 2.4.1. Class Separability

Training areas were delineated for each class (Eelgrass, Turbid Water, Highly Turbid Water, Clear Water) from the image mosaic on September 16 and

the image obtained on August 26, 2019. They were used to compute mean values for each class to assess the class separability in the case of the first 6 Landsat-8 bands (Figure 2.3), the Acolite variables (Figure 2.4), the vegetation indices (Figure 2.5), and the bathymetric ratios (Figure 2.6).

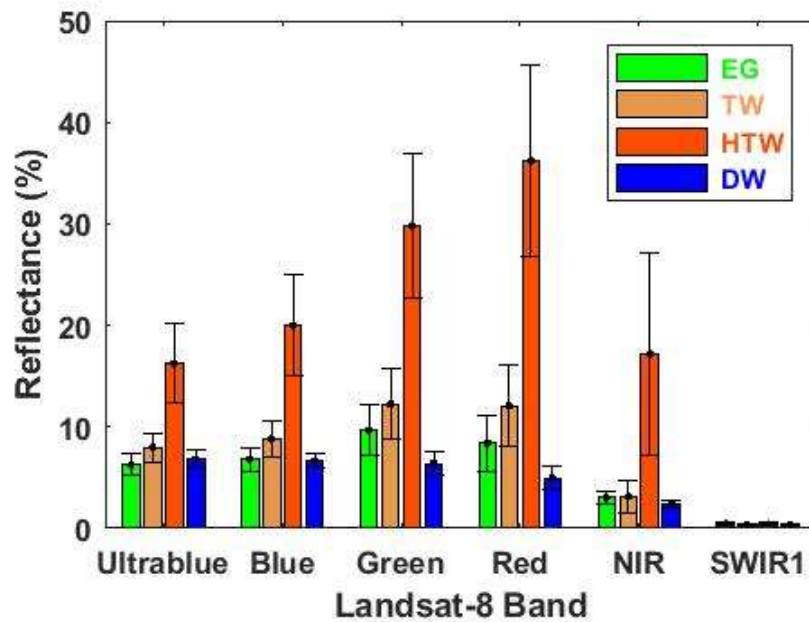


**Figure 2.3.** Mean reflectance values for each class for the first 6 Landsat-8 bands for both images

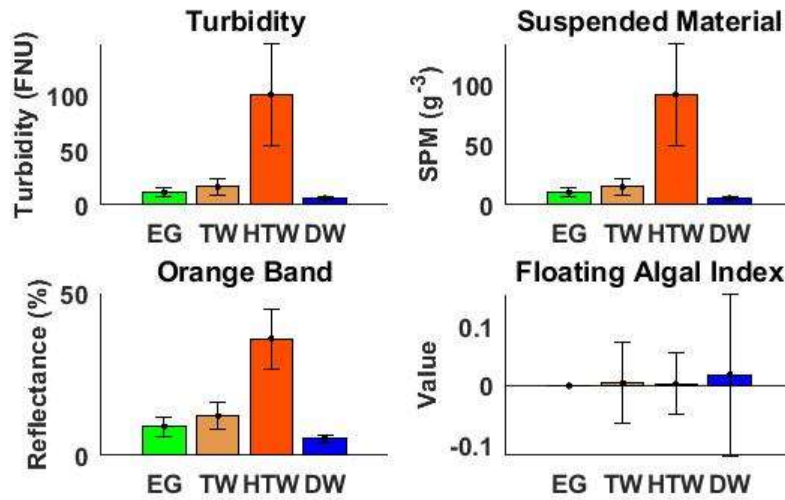


**Figure 2.4.** Mean values of the Acolite variables computed during the atmospheric correction for each class for both images

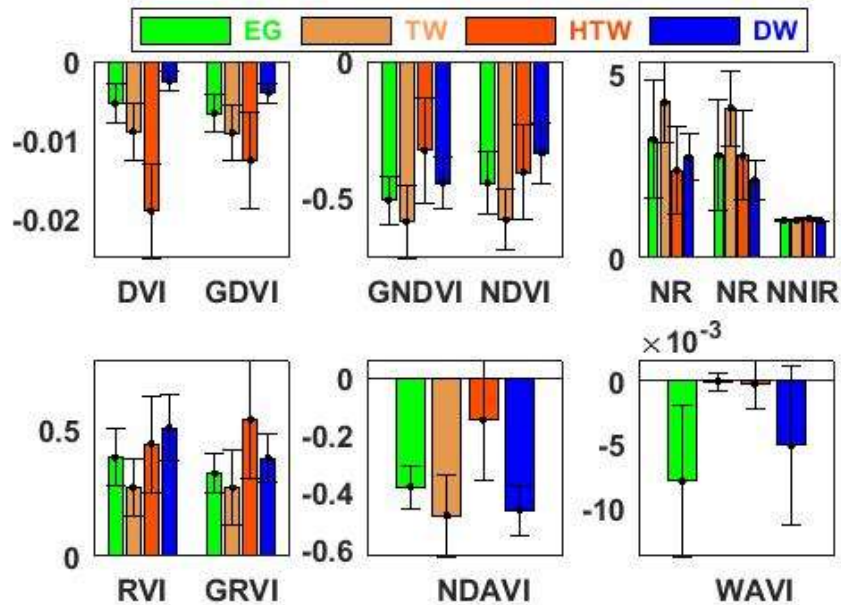


**Figure 2.5.** Mean values of the vegetation indices used in the study for each class for both images

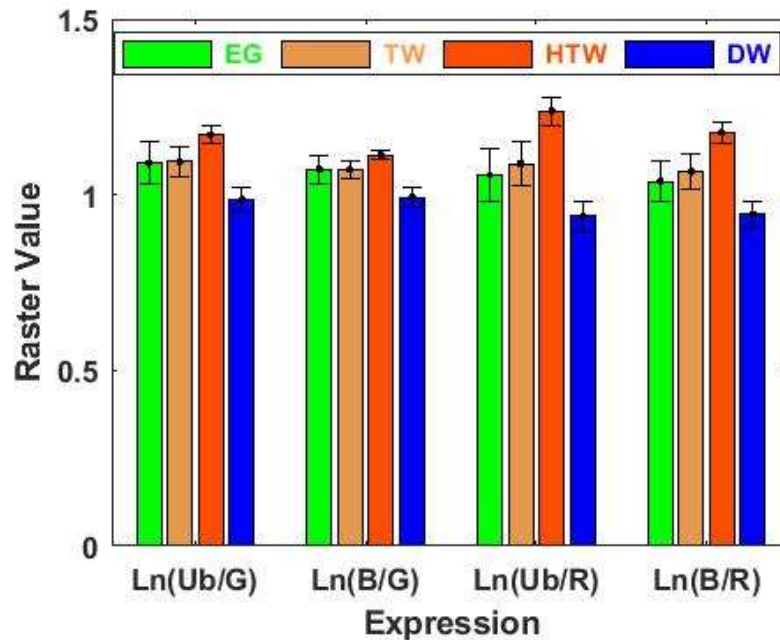


**Figure 2.6.** Mean values of each bathymetric ratio for each class for both images

The training areas of the September image were also used to assess the class spectral separability using the J-M distance computed with the six first Landsat-8 OLI bands (Table 2.4).

**Table 2.4.** J-M distances computed with the class training areas for the Landsat-8 OLI bands of the September image mosaic.

Class Code	EG	TW	HTW
TW	1.341	-	-
HTW	1.986	1.939	-
DW	1.388	1.674	1.999

## 2.4.2. Classification

The September 16 and August 26 images were then classified in R using the Random Forests classifier [41,42], using the six first Landsat-8 OLI bands and all variables listed in Table 2.3. The confusion matrix assessing the out-of-bag training areas within the classifier was combined for both images and is presented in Table 2.5. The classification accuracy is high, with an overall accuracy of 99.3%. The classified image is shown in Figure 2.7. Detailed maps were created at a scale of 1:250,000 around each of the main Cree coastal communities: Chisasibi (Figure 2.8), Wemindji (Figure 2.9), Eastmain (Figure 2.10), and Waskaganish (Figure 2.11).

**Table 2.5.** Confusion matrix for out-of-bag training pixels computed with the Random Forests classifier (bold values represent well-classified pixels).

<b>Class</b>	<b>EG</b>	<b>TW</b>	<b>HTW</b>	<b>CW</b>	<b>Total</b>	<b>UA (%)</b>
<b>EG</b>	<b>3139</b>	56	43	268	3506	89.5
<b>TW</b>	28	<b>33129</b>	78	197	33432	99.1
<b>HTW</b>	58	55	<b>96688</b>	65	96866	99.8
<b>CW</b>	69	274	74	<b>37866</b>	38283	98.9
<b>Total</b>	3294	33514	96883	38396	<b>172087</b>	
<b>PA (%)</b>	95.3	98.9	99.8	98.7		OA = 99.3%

The classified image was then assessed for accuracy by comparing the mapped eelgrass presence/absence to the field dataset provided by Hydro-

Quebec and the project's field research team. Points that were classified as turbid water were excluded from the validation analysis. We achieved an overall accuracy of 78.7% (Table 2.6). The eelgrass present class resulted in a User's accuracy of 84.2% and a Producer's accuracy of 87.3%, which are excellent considering the challenging environmental conditions.

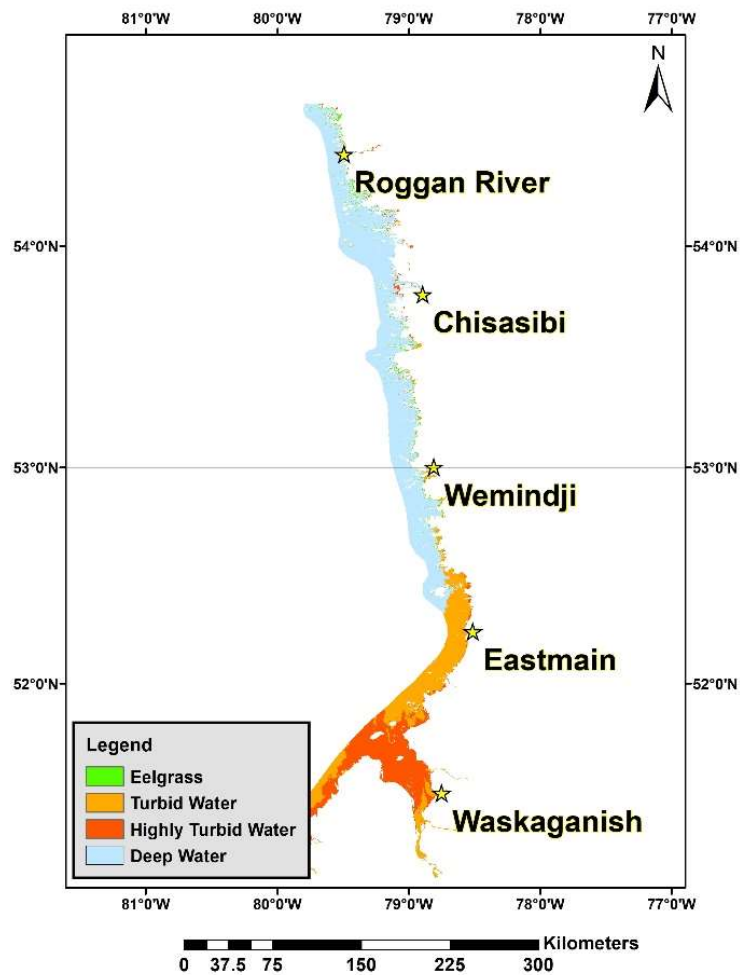


**Figure 2.7.** Classified image produced by applying the Random Forests classifier to both Landsat-8 OLI images

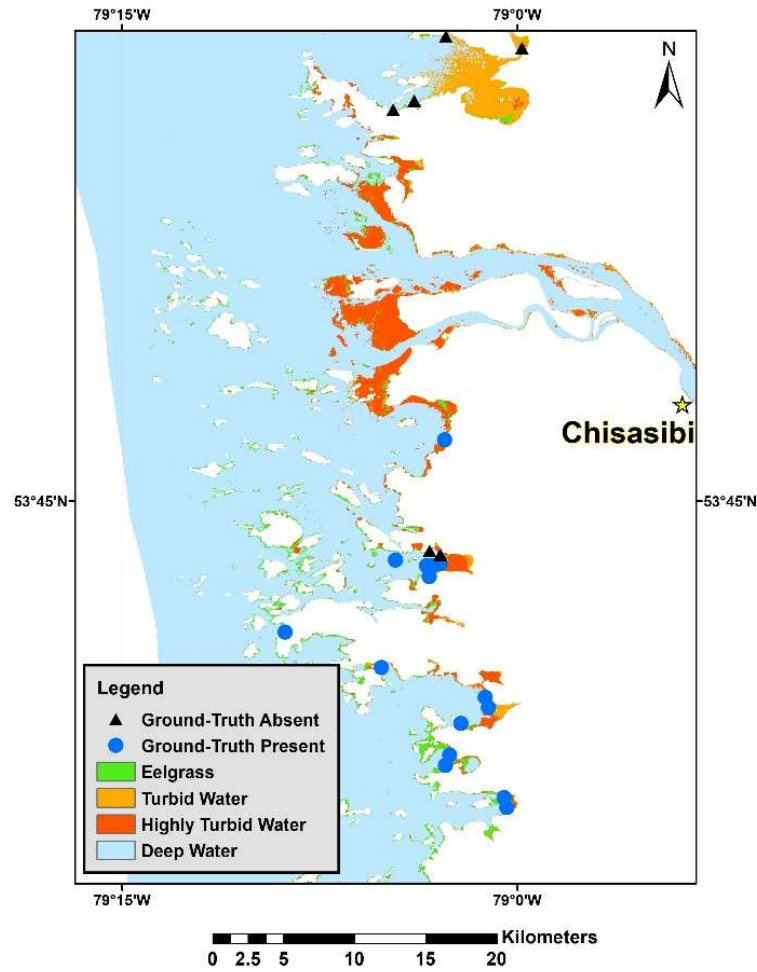


**Figure 2.8.** Classified image produced by applying the Random Forests classifier to both Landsat-8 OLI images for the coastline around Chisasibi

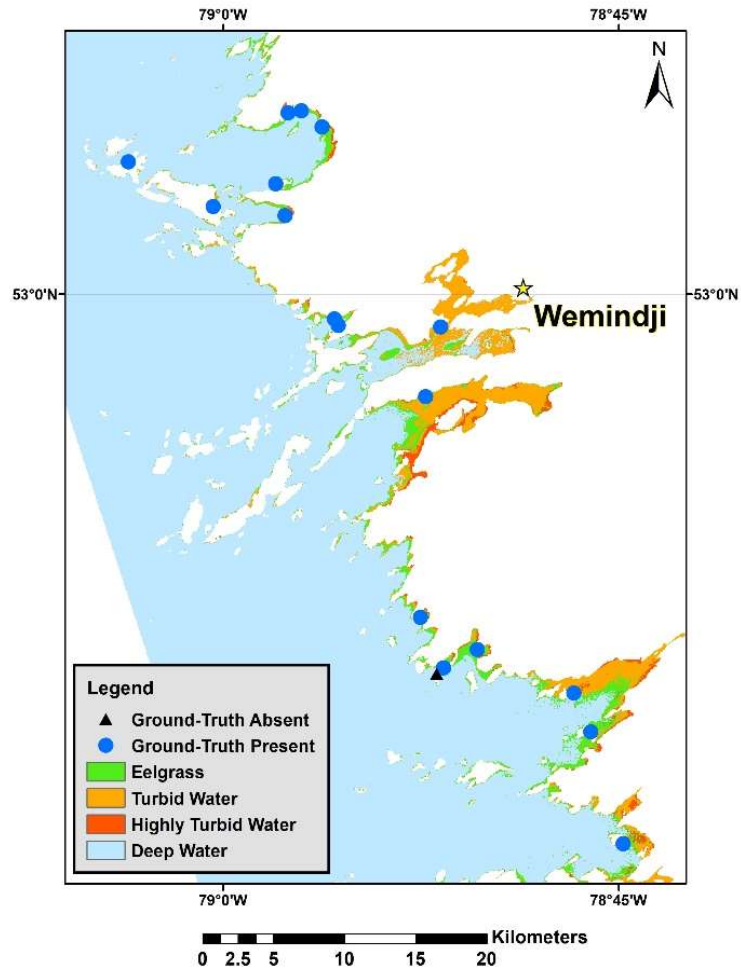


**Figure 2.9.** Classified image produced by applying the Random Forests classifier to both Landsat-8 OLI images outlining the coastline around Wemindji

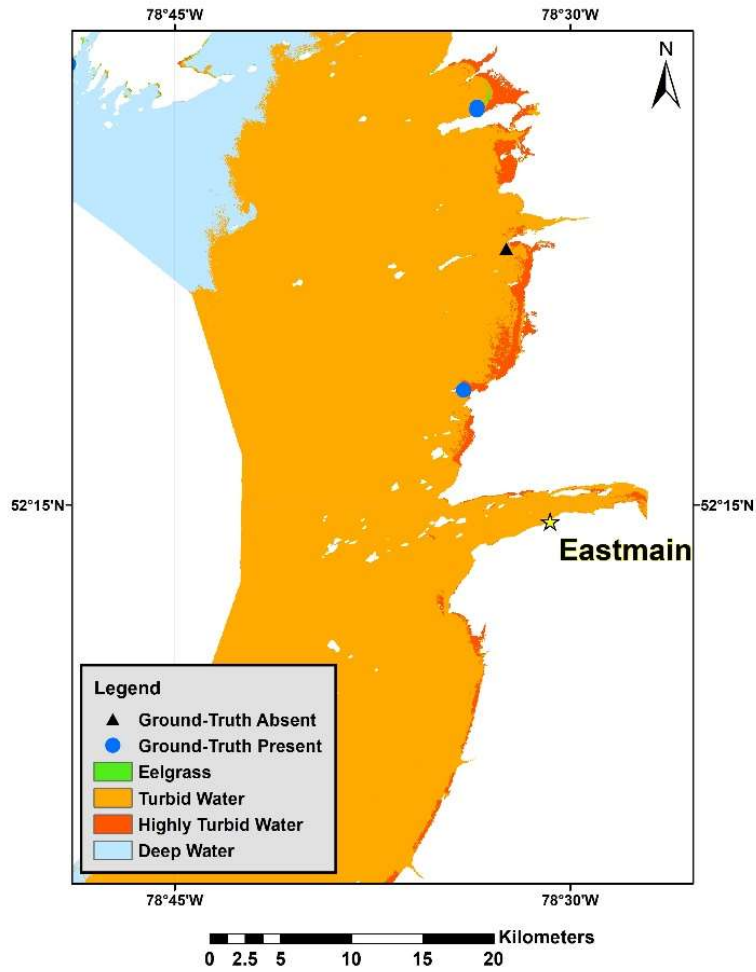


**Figure 2.10.** Classified image produced by applying the Random Forests classifier to both Landsat-8 OLI images outlining the coastline around Eastmain

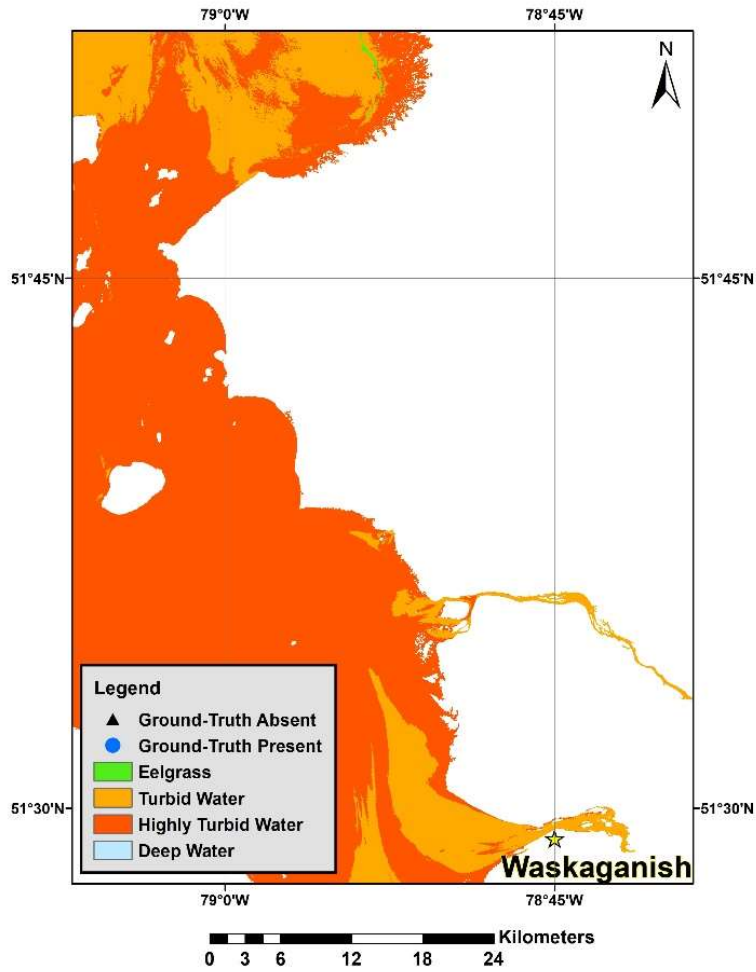


**Figure 2.11.** Classified image produced by applying the Random Forests classifier to both Landsat-8 OLI images outlining the coastline around Waskaganish

**Table 2.6.** Validation accuracies obtained by comparing field-based ground-truth sites with the classified image.

Class	Present	Absent	Total	UA (%)
Present	69	13	82	84.2
Absent	10	16	26	61.5
Total	79	29	108	OA = 78.7%
PA (%)	87.3	55.2		

## 2.5. DISCUSSION AND CONCLUSIONS

Our study presents preliminary results on combining local indigenous knowledge and Landsat-8 OLI imagery for mapping eelgrass beds in water with high turbidity. The imagery was atmospherically corrected using the Acolite software. We show that eelgrass can be spectrally distinguished from optically deep and turbid waters. The spectral signature of eelgrass was not shown to be detectable underneath suspended material in the water column since the red and green reflectance of turbid waters is dominated by particulate matter in the water column. The overall accuracy for the validation was 78.70%. Adding extra input layers to the Landsat-8 OLI reflectance bands improved the validation accuracy significantly. Decreasing or optimizing layers was shown not to increase the validation overall accuracy, and thus it is recommended to add these additional input layers to improve the accuracy of Landsat-8 classifications.

Our classified image mosaics did not show extensive eelgrass beds where it was possible to map them with the Landsat8-OLI imagery. Such observations agree with the Cree Land Users of Eeyou Istchee, who have noted steady declines in eelgrass coverage along the coast in the late 1980s and then a drastic decline in 1997-1998 [29]. Cree reported that since the decline in the late 1990s, the recovery of the eelgrass has been very slow. Such a study is, therefore, a good example of how local indigenous knowledge can be combined with Western science in a case study. Landsat-8 imagery, while providing exceptional temporal coverage, is limited in its spatial resolution.

The 30 m pixel size of Landsat-8 imagery limits the creation of training areas to only large beds that dominate the reflectance signal of a single pixel. Landsat-8 imagery may therefore not be suitable for classifying patchier eelgrass or smaller patches of turbid/clear water. The 30 m spatial resolution also makes an accurate location of the coastline difficult. This was not too much of an issue in James Bay, where optically shallow waters suitable for eelgrass extend far past the coastline-however it could present an issue if applied to a coastline with only a tiny strip (< 30 m width) of shallow enough water for eelgrass growth. Besides, while James Bay contains geographically large eelgrass beds, areas dominated by other types of submerged aquatic vegetation may have similar spectral characteristics. Therefore, this study framework may not be applicable for

locations where multiple submerged aquatic vegetation may encompass a geographic area larger than 30 m. While this study provided a framework for mapping eelgrass beds on a large spatial scale in turbid waters, more work should be done researching the accuracy of the Random Forests classifier on smaller spatial scales using higher resolution imagery. Sentinel-2 imagery could potentially offer bay-wide coverage at a 10 m resolution and should be explored as a high-resolution multispectral alternative. High-resolution hyperspectral imagery would be a suitable option for mapping sections of the Bay, but the unpredictable bay-wide turbidity could also make hyperspectral imagery acquisition costly or not feasible.

Lastly, substituting actual bathymetry data for the ratio decay algorithms used in this study may improve classification; however, in the absence of bathymetry data, the high spectral separability between deep clear water and eelgrass makes the bathymetric ratios a good alternative as a classifier input. Our classified image was validated against 108 points, and there is a need to add more validation points in further work.

## 2.6. REFERENCES

1. Olesen, B.; Krause-Jensen, D.; Marbà, N.; Christensen, P. Eelgrass *Zostera marina* in Subarctic Greenland: Dense Meadows with Slow Biomass Turnover in Cold Waters. *Marine Ecology Progress Series* **2015**, *518*, 107–121, doi:10.3354/meps11087.
2. Lalumière, R.; Messier, D.; Fournier, J.J.; Peter McRoy, C. Eelgrass Meadows in a Low Arctic Environment, the Northeast Coast of James Bay, Québec. *Aquatic Botany* **1994**, *47*, 303–315, doi:10.1016/0304-3770(94)90060-4.
3. Poursanidis, D.; Topouzelis, K.; Chrysoulakis, N. Mapping Coastal Marine Habitats and Delineating the Deep Limits of the Neptune’s Seagrass Meadows Using Very High-Resolution Earth Observation Data. *International Journal of Remote Sensing* **2018**, *39*, 8670–8687, doi:10.1080/01431161.2018.1490974.
4. Dignard, N.; Lalumière, R.; Reed, A.; Julien, M. Habitats of the Northeast Coast of James Bay **1991**. 27p.
5. Royer, M.-J.S. Eastern James Bay and the Cree. In *Climate, Environment and Cree Observations: James Bay Territory, Canada*; Royer, M.-J.S., Ed.; SpringerBriefs in Climate Studies; Springer International Publishing: Cham, 2016; pp. 35–61 ISBN 978-3-319-25181-3.
6. Prevett, J.P.; Lumsden, H.G.; Johnson, F.C. Waterfowl Kill by Cree Hunters of the Hudson Bay Lowland, Ontario. *ARCTIC* **1983**, *36*, 185–192, doi:10.14430/arctic2261.
7. Kollars, N.M.; Henry, A.K.; Whalen, M.A.; Boyer, K.E.; Cusson, M.; Eklöf, J.S.; Hereu, C.M.; Jorgensen, P.; Kiriakopolos, S.L.; Reynolds, P.L.; et al. Meta-Analysis of Reciprocal Linkages between Temperate Seagrasses and Waterfowl with Implications for Conservation. *Frontiers in Plant Science* **2017**, *8*, 2119, doi:10.3389/fpls.2017.02119.
8. Short, F.T.; Coles, R.G. Global Seagrass Research Methods. *Elsevier Science B.V., Amsterdam*. **2001**, 31–58.
9. Postlethwaite, V.R.; McGowan, A.E.; Kohfeld, K.E.; Robinson, C.L.K.; Pellatt, M.G. Low Blue Carbon Storage in Eelgrass (*Zostera marina*) Meadows on the Pacific Coast of Canada. *PLOS ONE* **2018**, *13*, e0198348, doi:10.1371/journal.pone.0198348.

10. Potouroglou, M.; Bull, J.C.; Krauss, K.W.; Kennedy, H.A.; Fusi, M.; Daffonchio, D.; Mangora, M.M.; Githaiga, M.N.; Diele, K.; Huxham, M. Measuring the Role of Seagrasses in Regulating Sediment Surface Elevation. *Scientific Reports* **2017**, *7*, 1–11, doi:10.1038/s41598-017-12354-y.
11. Marsh, J.H. James Bay Project. *The Canadian Encyclopedia* **2015**.
12. Milko, R. Potential Ecological Effects of the Proposed GRAND Canal Diversion Project on Hudson and James Bays. *ARCTIC* **1986**, *39*, 316–326, doi:10.14430/arctic2094.
13. Lalumière, R. *Étude de La Zostère Marine (Zostera marina) Sur La Côte Est de La Baie James - Été 1986*; **1986**. 112p.
14. Hydro-Quebec and GENIVAR Groupe Conseil Inc. *Environmental Monitoring of the La Grande Complex. Abridged Summary Report 1988-2000. Eelgrass Meadows of the Northeast Coast of James Bay.*; **2005**. 42p.
15. Hayeur, G. Summary of Knowledge Acquired in Northern Environments from 1970 to 2000. *Montreal: Hydro-Quebec* **2001**. 113p.
16. El-Sabh, M.I.; Koutitonsky, V.G. An Oceanographic Study of James Bay before the Completion of the La Grande Hydroelectric Complex. *ARCTIC* **1977**, *30*, 169–186, doi:10.14430/arctic2697.
17. Historic Landsat 5 Mission Ends | Landsat Science Available online: <https://landsat.gsfc.nasa.gov/article/historic-landsat-5-mission-ends/> (accessed on 24 June 2022).
18. Murphy, R. *Plant Fact Sheet EELGRASS Zostera marina Linnaeus Plant Symbol = ZOMA*; **2011**.
19. Bos, A.R.; Bouma, T.J.; de Kort, G.L.J.; van Katwijk, M.M. Ecosystem Engineering by Annual Intertidal Seagrass Beds: Sediment Accretion and Modification. *Estuarine, Coastal and Shelf Science* **2007**, *74*, 344–348, doi:10.1016/j.ecss.2007.04.006.
20. Wong, M.C.; Bravo, M.A.; Dowd, M. Ecological Dynamics of *Zostera marina* (Eelgrass) in Three Adjacent Bays in Atlantic Canada. *Botanica Marina* **2013**, *56*, 413–424, doi:10.1515/bot-2013-0068.
21. Joseph, V.; Schmidt, A.; Gregory, R. *Use of Eelgrass Habitats by Fish in Eastern Canada*. DFO Can. Sci. Advis. Sec. Res. Doc. 2012/138. Ii + 12p.

22. Kennedy, L.A.; Juanes, F.; El-Sabaawi, R. Eelgrass as Valuable Nearshore Foraging Habitat for Juvenile Pacific Salmon in the Early Marine Period. *Marine and Coastal Fisheries* **2018**, *10*, 190–203, doi:10.1002/mcf2.10018.
23. Macreadie, P.I.; Baird, M.E.; Trevathan-Tackett, S.M.; Larkum, A.W.D.; Ralph, P.J. Quantifying and Modelling the Carbon Sequestration Capacity of Seagrass Meadows – A Critical Assessment. *Marine Pollution Bulletin* **2014**, *83*, 430–439, doi: 10.1016/j.marpolbul.2013.07.038.
24. Seymour, N.R.; Miller, A.G.; Garbary, D.J. Decline of Canada Geese (*Branta canadensis*) and Common Goldeneye (*Bucephala clangula*) Associated with a Collapse of Eelgrass (*Zostera marina*) in a Nova Scotia Estuary. *Helgoland Marine Research* **2002**, *56*, 198–202, doi:10.1007/s10152-002-0112-4.
25. Short, F.; Carruthers, T.; Dennison, W.; Waycott, M. Global Seagrass Distribution and Diversity: A Bioregional Model. *Journal of Experimental Marine Biology and Ecology* **2007**, *350*, 3–20, doi: 10.1016/j.jembe.2007.06.012.
26. Martini, I.P. Chapter 7 Coastal Features of Canadian Inland Seas. *Elsevier Oceanography Series* **1986**, *44*, 117–142, doi:10.1016/S0422-9894(08)70900-0.
27. Nienhuis, P.; Groenendijk, A. Consumption of Eelgrass (*Zostera marina*) by Birds and Invertebrates: An Annual Budget." *Marine Ecology Progress Series*, **1986**, *29(1)*, 29–35. *JSTOR*, <http://www.jstor.org/stable/24817532>. (accessed on 16 June 2020).
28. COMEX Report on the Public Consultations Held in November 2012 Following Implementation of Hydro-Quebec's Eastmain-1-A and Sarcelle Powerhouses and Rupert Diversion Project **2013**. 238p.
29. CONSORTIUM GENIVAR-WASKA *Centrales de l'Eastmain-1-A et de La Sarcelle et Dérivation Rupert. Suivi de La Zostère Marine de La Côte Nord-Est de La Baie James.*; **2017**. Vol. 1. 85p.
30. O'Neill, J.D.; Costa, M. Mapping Eelgrass (*Zostera marina*) in the Gulf Islands National Park Reserve of Canada Using High Spatial Resolution Satellite and Airborne Imagery. *Remote Sensing of Environment* **2013**, *133*, 152–167, doi: 10.1016/j.rse.2013.02.010.
31. Reshitnyk, L.; Costa, M.; Robinson, C.; Dearden, P. Evaluation of WorldView-2 and Acoustic Remote Sensing for Mapping Benthic Habitats in Temperate Coastal Pacific Waters. *Remote Sensing of Environment* **2014**, *153*, 7–23, doi: 10.1016/j.rse.2014.07.016.

32. Taha, W.; Bonneau-Lefebvre, M.; Cueto Bergner, A.; Tremblay, A. Evolution from Past to Future Conditions of Fast Ice Coverage in James Bay. *Frontiers in Earth Science* **2019**, *7*, doi:10.3389/feart.2019.00254.
33. Leblanc, M.L., O'Connor, M. I., Kuzyk A., Z., Noisette, F., del Giorgio, P., Leblon, B., LaRocque, A., Humphries, M. 2022. Limited recovery following the greatest seagrass decline in subarctic eastern Canada, *Global Change Biology* (submitted).
34. Vanhellemont, Q.; Ruddick, K. Atmospheric Correction of Metre-Scale Optical Satellite Data for Inland and Coastal Water Applications. *Remote Sensing of Environment* **2018**, *216*, 586–597, doi: 10.1016/j.rse.2018.07.015.
35. Vanhellemont, Q. Adaptation of the Dark Spectrum Fitting Atmospheric Correction for Aquatic Applications of the Landsat and Sentinel-2 Archives. *Remote Sensing of Environment* **2019**, *225*, 175–192, doi: 10.1016/j.rse.2019.03.010.
36. Sen, R.; Goswami, S.; Chakraborty, B. Jeffries-Matusita Distance as a Tool for Feature Selection. In Proceedings of the 2019 International Conference on Data Science and Engineering, ICDSE 2019; Institute of Electrical and Electronics Engineers Inc., September 1, **2019**. 15–20.
37. Nechad, B.; Ruddick, K.G.; Park, Y. Calibration and Validation of a Generic Multisensor Algorithm for Mapping of Total Suspended Matter in Turbid Waters. *Remote Sensing of Environment* **2010**, *114*, 854–866, doi: 10.1016/j.rse.2009.11.022.
38. Dogliotti, A.; GosGossen.; Vanhellemont, Q.; Ruddick, K. Detecting and Quantifying a Massive Invasion of Floating Aquatic Plants in the Río de La Plata Turbid Waters Using High Spatial Resolution Ocean Color Imagery. *Remote Sensing* **2018**, *10*, 1140, doi:10.3390/rs10071140.
39. Castagna, A.; Simis, S.; Dierssen, H.; Vanhellemont, Q.; Sabbe, K.; Vyverman, W. Extending Landsat 8: Retrieval of an Orange Contra-Band for Inland Water Quality Applications. *Remote Sensing* **2020**, *12*, 637, doi:10.3390/rs12040637.
40. Stumpf, R.P.; Holderied, K.; Sinclair, M. Determination of Water Depth with High-Resolution Satellite Imagery over Variable Bottom Types. *Limnology and Oceanography* **2003**, *48*, 547–556, doi: 10.4319/lo.2003.48.1\_part\_2.0547.
41. Breiman, L. Random Forests. *Machine Learning* **2001**, *45*, 5–32, doi:10.1023/A:1010933404324.

42. Horning, N. *Random Forests: An Algorithm for Image Classification and Generation of Continuous Fields Data Sets*; **2010**.
43. Mograne, M.; Jamet, C.; Loisel, H.; Vantrepotte, V.; Mériaux, X.; Cauvin, A. Evaluation of Five Atmospheric Correction Algorithms over French Optically Complex Waters for the Sentinel-3A OLCI Ocean Color Sensor. *Remote Sensing* **2019**, *11*, 668, doi:10.3390/rs11060668.
44. Warren, M.A.; Simis, S.G.H.; Martinez-Vicente, V.; Poser, K.; Bresciani, M.; Alikas, K.; Spyrakos, E.; Giardino, C.; Ansper, A. Assessment of Atmospheric Correction Algorithms for the Sentinel-2A MultiSpectral Imager over Coastal and Inland Waters. *Remote Sensing of Environment* **2019**, *225*, 267–289, doi: 10.1016/j.rse.2019.03.018.

**CHAPTER 3: USE OF LANDSAT IMAGERY TIME SERIES AND RANDOM  
FORESTS CLASSIFIER TO RECONSTRUCT EELGRASS BED  
DISTRIBUTION MAPS IN EEYOU ISTCHEE**

**3.1. ABSTRACT**

The eastern coastline of James Bay is known to be home to sizeable beds of eelgrass (*Zostera marina* L.), which thrive in the bay's shallow, subarctic waters. The region was subjected to substantial hydroelectric dams, large fires, and other human activities in the past half-century. To assess the impact of these factors on eelgrass beds, a historical reconstruction of eelgrass bed distribution was performed from images acquired by Landsat-5 Thematic Mapper in 1988, 1991, and 1996, and images of the Landsat-8 Operational Land Imager (OLI) in 2019. All the images were classified using the Random Forests classifier and assessed for accuracy each year on a bay-wide scale using an independent field validation dataset. The validation data were extracted from eelgrass bed maps that were established from aerial photos and field surveys in 1986-1987, 1991-1992, and 1995-1996 and from a field survey in 2019. The overall validation accuracy of the classified images (between 72% and 85%) showed good agreement with the other datasets for most locations, making it possible to use satellite imagery for detecting past changes to eelgrass distribution within a bay. The classified images of 1988 and 1996 were also compared to aerial photos taken at close years

at ten sites to determine their capability to assess the shape and presence of small eelgrass beds. Such a comparison revealed that the classified images accurately portrayed eelgrass distribution even at finer scales.

### 3.2. INTRODUCTION

*Zostera marina* L. (commonly referred here to as eelgrass) is a seagrass species that grows in shallow and intertidal habitats throughout the northern hemisphere and provides valuable ecosystem services to both terrestrial and aquatic ecosystems [1–3]. It has historically been found to occur along the eastern coastline of James Bay, i.e., the southernmost embayment of Hudson Bay, which offers suitable habitat for eelgrass growth (i.e., low tidal slope, protection from wind and wave action, suitable substrate) [4,5]. It is a fundamental part of the region's various coastal ecosystems as it serves as a source of shelter for fish and invertebrates, as well as an essential source of food for migratory waterfowl [1,6]. In James Bay, eelgrass has a slow vegetative and reproductive rate, similar to Arctic macroalgae species [4,7]. Its growth is influenced by several environmental factors, including ice, wind, wave action, substrate composition, and irradiance [5,8].

James Bay is referred to as Eeyou Istchee by the Cree inhabitants who have historically resided in the region. The Cree consistently rely on geese hunting as a primary form of subsistence [9,10]. Species of particular importance to the Cree include the Canadian Goose (*Branta canadensis*) and the Atlantic Brant (*Branta bernicla*), both of which are documented to feed on eelgrass in the region [10,11]. For this reason, knowledge about the health and distribution of eelgrass in the bay is of critical importance for the Cree. The Cree Land Users of Eeyou Istchee have noted steady declines in eelgrass coverage along the coast in the late 1980s and then a drastic decline in 1997-1998 [12]. They have also reported that since the decline in the late 1990s, eelgrass recovery has been very slow, and the eelgrass currently observed in some areas seems unhealthy (e.g., shorter, less dense, discolored) [13], which has in, in turn, has had an effect on the predictability of geese to appear around documented feeding areas [13].

In 1974, the Canadian Wildlife Service attempted the first large-scale mapping effort of eelgrass in James Bay, utilizing black and white aerial photography to create a distribution map at a scale of 1:125,000 [14]. All major beds along the coast were recorded and generalized spatially into one of four distribution classes based on estimated percent cover. This was the only large-scale analysis of eelgrass distribution in the bay before the construction of most of the hydroelectric dams. In 1987, the James Bay Energy Corporation deemed it

necessary to update the map with distribution changes over the past 12 years using color aerial photography at a scale of 1:10,000 as well as field validation using divers to ascertain the limit of eelgrass distribution [15] This exercise was repeated in 1991 and 1996, and distribution maps were derived from analysis of aerial photos for each of these years. Some aerial photographs were used to monitor changes in the detectable limit of continuous and discontinuous eelgrass beds at 14 sites in 1986 and 1996 [16]. In addition to the large-scale mapping, Hydro-Quebec initiated six permanent sampling stations in their monitoring effort, nearly all of them around Chisasibi, to estimate the impact of the hydrological changes in the bay's effect on eelgrass (since the most pronounced impact would be around Chisasibi) [16,17]. The results of the 1996 investigation concluded that eelgrass distribution in the bay had not changed drastically and that most of the hydrological changes due to the building of the La Grande complex would affect eelgrass in winter when the plant was in a physiologically dormant state [18]. In 1996, Hydro-Quebec concluded that regular analysis of the bay-wide distribution of eelgrass was unnecessary, and irregular monitoring was carried out from that point onward. In 1998, there was a significant, documented die-off of eelgrass that has since lacked a clear explanation. Reports indicate that eelgrass beds have been recovering [13,18] but have not managed to rebound back to the level they existed at before this event [19].

These inconsistencies in data collected by Hydro-Quebec outline the need for continuous and independent monitoring of eelgrass distribution along the Eeyou Istchee coastline. Due to the many limitations on researchers to perform field surveys in James Bay (i.e., harsh winter conditions, the extent of coastline, shallowness of coastline limiting the operating capacity of ships, etc.), satellite image analysis presents the best option for cost-effective, routine monitoring of the entire extent of the coast. Previous attempts to map eelgrass distribution along the bay using satellite imagery have been scarce and varied in their methodology. Kennedy et al. (2009) conducted a preliminary eelgrass change detection analysis using Landsat-5 TM images acquired between 1988 and 2003. They also tested multiple approaches to produce eelgrass bed maps from the images. While they could detect a change in the eelgrass distribution using image differentiation techniques, they could not correctly classify the images [20]. A team from the University of New Hampshire and Stantec consulting firm set out to classify eelgrass extent along the coast utilizing high-resolution imagery. In a first study [21], an unsupervised classifier (ISOCCLUS) was applied to mosaics made with WorldView-2 and RapidEye images acquired in 2012 and 2013. The images were not subjected to atmospheric corrections. They achieved an overall validation accuracy for the presence/absence of eelgrass of 72.7% when comparing the resulting classified image to 77 ground-truth points collected in

the summer of 2016. In a second study [22,23], PlanetScope images acquired in 2017 were subjected to atmospheric corrections using AtmosC, based on an outdated atmospheric correction algorithm [24] and classified with a supervised classifier (Maximum Likelihood Classifier). As part of this research, the authors achieved an overall validation accuracy for the presence/absence of eelgrass of 73.7% when comparing the resulting classified image to 209 ground-truth points collected in the summers of 2016, 2017, and 2018.

In this study, we aim to present a mapping approach for evaluating the distribution of eelgrass along the eastern coast of James Bay utilizing both freely available imagery from the Landsat-5 Multispectral Instrument (MSI) and Landsat-8 Operational Land Imager (OLI), in conjunction with preexisting field data collected by Hydro-Quebec. Images were classified using a non-parametric supervised classifier (Random Forests) that was shown to outperform the Maximum Likelihood classifier\_in many eelgrass mapping studies (e.g., (Traganos et al. 2018, Fethers et al. 2018, Aarts et al., 2020) [25–27]. The classified images were assessed for accuracy on a bay-wide scale using an independent field validation dataset for each year. The validation data were extracted from eelgrass bed maps established from aerial photos and HQ field surveys in 1986-1987, 1991-1992, and 1995-1996 [16] and a field survey performed by both HQ and the CCHRP field team in 2019. The classified images from 1988 and 1996

were then directly compared to the aerial photo-derived maps at several locations in the area to ascertain the ability of the classified multispectral satellite imagery to effectively map the shape of more localized eelgrass beds. The accuracy, limitations, and applicability of our classified image maps are discussed, and recommendations are made for a consistent future eelgrass distribution monitoring approach. The present study is part of the James Bay Coastal Habitat Comprehensive Research Program (JBCHCRP), a Cree-driven project aiming to combine Cree's traditional knowledge with Western science to understand better environmental changes in the coastal ecosystems and ecosystem services of Eeyou Istchee.

### **3.3. MATERIALS AND METHODS**

#### **3.3.1. Study Area**

The study area is located on the western coastline of Eeyou Istchee (or the eastern coastline of James Bay in western Quebec (Figure 1). We considered only two zones of the whole coastline where historical maps existed because they were used as ground-truth data for the classification. The first zone is north of Chisasibi and spans from 54° 0' Latitude N. to about 54° 40' Latitude N. The second one is south of Chisasibi and spans from 53° 20' Latitude N. to 53° 45'



available. Images selected were prioritized according to two criteria: (i) images were as free of cloud cover as possible; (ii) images were acquired as close as possible to peak eelgrass biomass season (late summer). Due to the limited amount of cloud and ice-free scenes available that covered the full extent of the coastline, tidal level was not accounted for when selecting imagery. In addition, tidal data for this region was not consistently until the 21<sup>st</sup> century, so accurate tidal measurements do not exist for the historical study period (1988 – 1996). Imagery from the Landsat-5 Thematic Mapper (Collection-2) was acquired as close as possible to the years of the aerial photos and field surveys used for establishing the historical maps, i.e., 1986-1987, 1991-1992, and 1995-1996 [16]. For the 1991-1992 and 1995-1996 historical data, cloud-free Landsat-5 TM imagery was available for the entire extent of the area covered by the distribution maps derived from the aerial photographs in 1991 and 1996, respectively. For the 1986-1987 historical data, cloud-free imagery was unavailable for the summer of 1985, 1986, and 1987. Fortunately, in the summer of 1988, one cloud-free image was acquired for most of the eastern coastline. However, the northernmost part of the study area was covered by clouds for this image. We also used Landsat-8 Operational Land Imager (OLI) (Collection-2) imagery in 2019 that covers both zones and coincides with the 2019 summer field survey by the JBCHCRP team.

**Table 3.1.** List of the images used in the study and associated date and cloud cover

Sensor	Image Acquisition Date	Image Path / Row	Scene Cloud Cover (%)
Landsat-5 MSI	24-Jul-1988	020 / 022	26
		020 / 023	2
	17-Jul-1991	020 / 022	7
		020 / 023	48
	16-Sep-1996	020 / 022	0
		020 / 023	0
Landsat-8 OLI	16-Sep-2019	020 / 022	0
		020 / 023	0

### 3.3.3. Other Data

For the 1988, 1991, and 1996 classifications, the ground-truth data were extracted from eelgrass distribution maps established over the two zones based on aerial photo interpretation, helicopter-based aerial surveys, and snorkeling/diving survey in the summers of 1986-87, 1991-1992, and 1995-1996 (Figure 3.2.) [16,18]. This dataset was used to train the classifier and validate the resulting classified images. For the maps to be usable, they were first digitized and georeferenced using ESRI ArcMap’s Georeferencing toolbox, which allows the user to compare point locations between the target map and reference image. Due to changes in tide between each image, as well as potential coastline changes due to the high rates of the isostatic rebound in the region [28] each historical map was georeferenced using its respective year’s Landsat-5 MSI imagery as the reference image. Once each map was digitized, the distribution polygons were

traced manually and saved as polygon shapefile data. For the 2019 classification, the field data were acquired the same year via a snorkeling/diving survey, and eelgrass presence/absence was recorded using a GPS at each evaluation site. Each point location was saved, and the dataset was converted to a point shapefile dataset. This dataset was only used for validating the classified image. To account for varying survey extents by Hydro-Quebec between each of their distribution maps, we limited our study area to only where survey extent was the same during all three years North of Chisasibi (northern zone) and South of Chisasibi (southern zone), except for the 1988 southern zone (Figure 3.2).. To account for this, the 1988 image was assessed for accuracy only as far south as the published distribution maps for Hydro-Quebec.

	1986	1991	1995
--	------	------	------

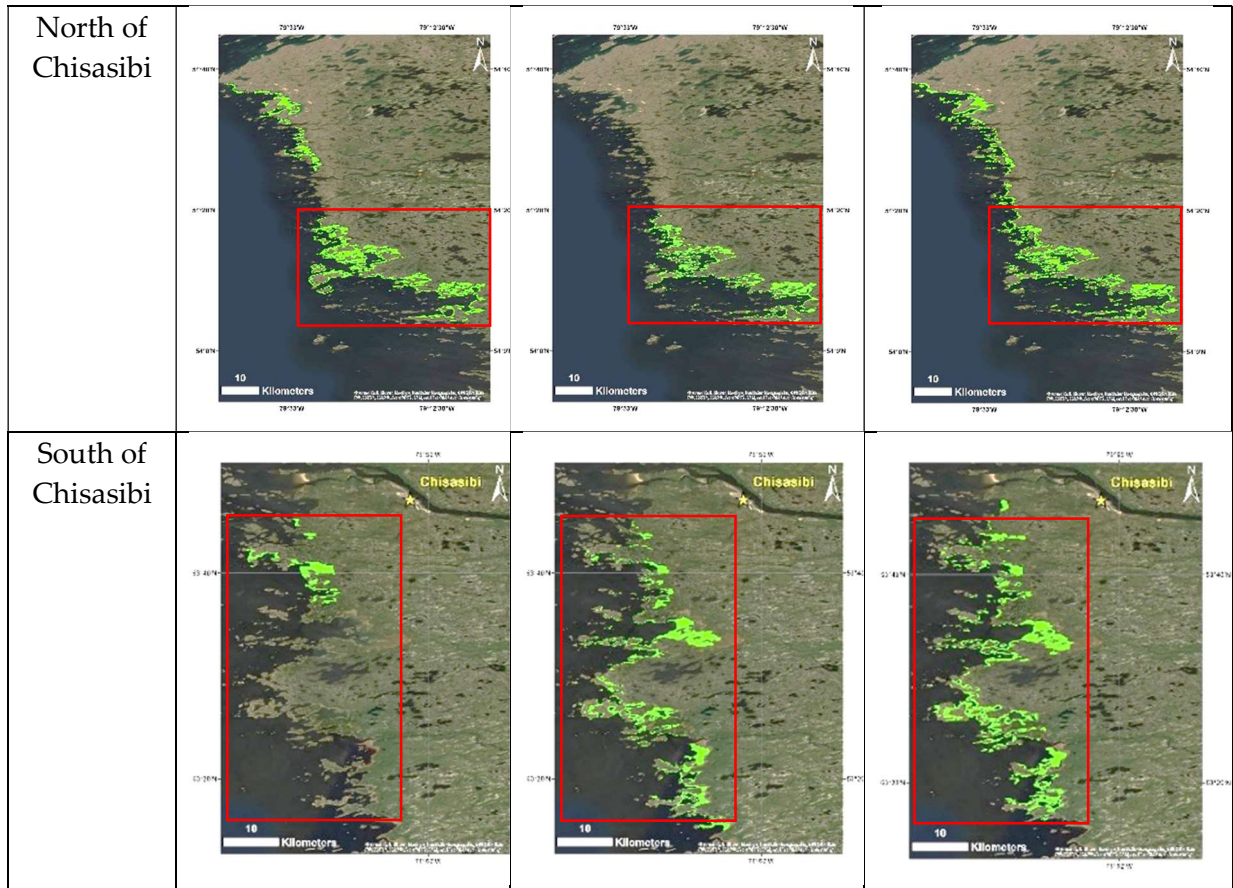


**Figure 3.2.** Digitized historical eelgrass bed distribution maps overlaid over a Google Earth image as a function of the year. Data outside of the red box was excluded from the study area due to varying survey extents.

Since the eelgrass grows in areas of less than 5 m water depth, there is a need to define these areas. However, bathymetric data are unavailable for the bay. Therefore, we estimated a water depth with a digital terrain model (DTM) that was extracted from the Shuttle Radar Topographic Mission (SRTM) data from the United States Geological Survey (<https://earthexplorer.usgs.gov/>). The SRTM DTM consists of one arc-second global grid (approximately 30m×30 m)

produced from resampling of the original three arc-second grid of elevation data (about 90m by 90 m) collected by the Endeavour Space Shuttle between 11 and 22 February 2000 (Farr et al., 2007). The DEM has a resolution of 1m in the z-direction (elevation), recorded in m relative to Mean Sea Level (MSL).

#### **3.3.4. Image Processing**

To create suitable imagery for detecting and monitoring submerged aquatic vegetation change, Level-1 Landsat imagery must be corrected for atmospheric effects (i.e., aerosol scattering, sun glint, etc.) before analysis [29]. Acolite, a free, open-source atmospheric correction software created by the Royal Belgian Institute of Natural Sciences, was selected due to its ease of use across multiple types of multispectral satellite imagery, as well as its capability to perform numerous steps of processing, such as the merging of adjacent imagery, sun glint correction, and production of derived imagery layers, such as turbidity [30–32]. Acolite was also shown to perform better than other similar freely-available atmospheric correction software in turbid coastal waters for atmospheric correction of multispectral satellite imagery [33–35]. Acolite presents the user with multiple optional parameters for computation during the atmospheric correction, including sun glint correction and image merging, utilized for each image year[36]. An example of a setting file that outlines the parameters set during Acolite atmospheric correction is available in this thesis's

Appendix. The image type utilized in the process was the water reflectance image, created by Acolite using a SWIR-based land mask [37]. Once the Acolite processing was completed, all subsequent image processing was performed in PCI Geomatica Banff.

The atmospherically corrected images produced by Acolite were inputted into the RF classifier. We only used the band images listed in Table 3.2. Additional layers were added to each classification to bolster the RF classifier performance. The first layer is the Turbidity, expressed in Formazin Nephelometric Units (FNU) computed by Acolite [32]. Other layers include eleven vegetation indices (Table 3) that were selected based on work by Forsey et al. (2020) [38] and bathymetric ratios, which are based on a ratio decay algorithm designed for evaluating satellite-derived bathymetry [39]. Since there are few reliable bathymetry sources for James Bay and bathymetry has an obvious effect on eelgrass growth, two “relative depth” layers were created from the DTM as follows. The elevations of the land mass were transformed into a slope layer that was the extent to the water area. The resulting slope layer was converted to an elevation layer as a function of the coast distance to estimate the water depth. This allows the ability to create additional input features for the classifier, defining the deep water zone (water depth higher than 5 m) and the shallow water zone with a water depth of less than 5m. Both zones were only delineated

where there were no islands along the coast. The island zone was considered a shallow water zone.

**Table 3.2.** Wavelengths of the Landsat-5 and Landsat-8 bands of the images used in the study

Band Name	Landsat-5 TM	Landsat-8 OLI
	Wavelength (nm)	Wavelength (nm)
Coastal		430 - 450
Blue	450 - 520	450 - 510
Green	520 - 600	530 - 590
Red	630 - 690	640 - 670
NIR	760 - 900	850 - 880
SWIR1	1550 - 1750	1570 - 1650
SWIR2	2080 - 2350	2110 - 2290

**Table 3.3.** Vegetation indices and bathymetric ratios considered in our study.

Variable	Layer Name	Formula <sup>(1)</sup>	Reference
DVI	Difference vegetation index	$NIR - R$	[40]
GDVI	Green difference vegetation index	$NIR - G$	[41]
GNDVI	Green normalized difference vegetation index	$(NIR - G) / (NIR + G)$	[42]
GRVI	Green ratio vegetation index	$NIR / G$	[41]
NDAVI	Normalized difference aquatic vegetation index	$(NIR - B) / (NIR + B)$	[43]
NDVI	Normalized difference vegetation index	$(NIR - R) / (NIR + R)$	[44]
NG	Normalized green vegetation index	$G / (NIR + R + G)$	[41]
NNIR	Normalized near-infrared vegetation index	$NIR / (NIR + R + G)$	[41]
NR	Normalized red vegetation index	$R / (NIR + R + G)$	[41]
RVI	Red ratio vegetation index	$NIR / R$	[45]
WAVI	Water-adjusted vegetation index	$1.5 * (NIR - B) / (NIR + B + 0.5)$	[43]
Coastal/Green	Bathymetric Ratio (Coastal/Green)	$Ln(Coastal)/Ln(Green)$	[39]
Coastal/Red	Bathymetric Ratio (Coastal/Red)	$Ln(Coastal)/Ln(Red)$	[39]
Blue/Green	Bathymetric Ratio (Blue/Green)	$Ln(Blue)/Ln(Green)$	[39]
Blue/Red	Bathymetric Ratio (Blue/Red)	$Ln(Blue)/Ln(Red)$	[39]
RD1	Relative Depth- 1	Shallow water of less than 5 m deep	This paper
RD2	Relative Depth- 2	Deep water of more than 5 m deep	This paper

<sup>(1)</sup> B = reflectance in the blue band; G = reflectance in the green band; NIR = reflectance in the near-infrared band; R = reflectance in the red band; CA = reflectance in the coastal / aerosol band

### 3.3.5. Model Training Data

The Random Forests classifier used in our study is a supervised classifier that requires training data in polygon shapefile format [46]. Since water conditions in the bay (including turbidity, ice, wind, wave action, etc.) can be highly variable in this region based on runoff or time of year [47], water conditions could not be guaranteed to be similar across the year and training areas had to be individually created for each of the respective classification years. Five classes were considered for each training set: Eelgrass, Low Turbidity Water, High Turbidity Water, Bare Seafloor, and Deep Water. The number of training pixels created for each class and classification year is displayed in Table 3.4. For every year, each set of training data was created in an iterative process until the final image product, and the spectral separability between classes computed as a J-M distance was deemed to be satisfactory

**Table 3.4.** Number of training pixels used to train the Random Forests model according to the year and class

<b>Class</b>	<b>1988</b>	<b>1991</b>	<b>1996</b>	<b>2019</b>
Eelgrass	4604	3028	4012	3225
Low Turbidity	9234	38501	14568	7795
High Turbidity	1962	417	3744	2474
Seafloor	2721	1034	1726	905
Deep Water	119800	56024	79992	106253
Total	138321	99004	104042	120652

Training areas for the classified historical imagery (1986-1987, 1991-1992, and 1995-1996) were extracted from the distribution maps of Figure 3.2 derived from aerial photos as well as by photointerpretation of the multispectral imagery. The Eelgrass class was created where field surveys recorded eelgrass presence in that respective year or where large eelgrass beds were visible on the multispectral satellite imagery. Where field data were derived from the historical distribution maps, eelgrass training polygons were created in areas with large, high-density eelgrass beds recorded on the map. Priority for creating training polygons for the eelgrass class was given to areas of consistent eelgrass presence or locations where eelgrass presence was recorded for each of the three historical years. Likewise, no deep water polygons were created over pixels containing eelgrass on any historical distribution maps. The low and high turbid water training polygons were created solely based on photo-interpretation of the RGB composites, regardless of the year of classification. The low turbid water has a distinctly grayish color. The high turbid water has a distinctly brownish color. This class is also well defined in the Turbidity layer computed by Acolite. Bare seafloor was defined as pixels close to the shoreline, where the seafloor was visible, and the dominant reflectance signature of the pixels was not indicative of submerged aquatic vegetation. The Deep Water class was defined by water pixels that did not appear to have a distinct hue (i.e., appearing dark blue or

black on the RGB multispectral satellite imagery), were not close to shore, and where no presence of eelgrass was indicated from the historical data.

For 2019, polygon training data for the Eelgrass and Deep Water classes were derived entirely from photointerpretation of the Landsat-8 imagery, and field data acquired during this year were used for validating the classified image. The Eelgrass class for this year was defined where the reflectance of near-shore pixels appeared to be dominated by submerged aquatic vegetation, usually expressed by a strong green hue in the RGB imagery, especially if it was in an area of documented or otherwise established eelgrass presence such as the locations of the field sites. The point field dataset used to validate the 2019 model was not used for guiding the creation of training areas for these years since that would deprecate the ability of these data points to validate the 2019 classified image.

### **3.3.6. Image Classification**

Once each image classification's respective training dataset was completed, the classifications were carried out using the Random Forests classifier [48,49] using an R script designed for the classification of multispectral satellite imagery [46], with the training areas being re-assessed based on the resulting classification in an iterative process. Once the resulting training areas achieved an acceptable level of accuracy, a final classification was then

performed for each year, and statistics from each classification were recorded. The resulting classified images were filtered using a SIEVE filter in PCI Geomatica, which filters out smaller unconnected polygons to reduce the impact of small misclassifications on overall accuracy. The SIEVE filter filtered out all pixels connected to less than seven other pixels with the same value, using the basis of eight connectedness [50]

### **3.3.7. Accuracy Assessment**

Each classified image was assessed for accuracy using two metrics; the first metric was classification accuracy measured using a subset training of the training data within the RF classifier, and the second was a randomly generated dataset derived from the ground-truth data for each classification year. For the historical classifications (1988, 1991, and 1996), validation points were randomly generated from each respective image classification and validated against the historical distribution maps, which in this context functioned as ground-truth data. A set of 100 points was randomly generated for each of the two zones (North and South of Chisasibi) for all the classified images. The points were generated in ArcMap by using the “create accuracy assessment points” tool. Half of the points were generated on pixels where eelgrass was not classified (i.e., pixels classified as bare seafloor or deep water), while the other half were generated on pixels classified as eelgrass. These points were then manually

assessed to determine whether they matched the data shown on the historical distribution maps. If a pixel classified as EP was not within the limits of the eelgrass beds defined by the distribution map (or within reasonable approximation to the photointerpreter), that point (and therefore pixel) was considered incorrectly classified. Similarly, a point considered as EA was only correctly classified if it was NOT located on or directly next to an eelgrass bed, as defined by the associated historical distribution map. The results were displayed in a confusion matrix. For the 2019 validation data, ground-truth points from the 2019 field surveys of Hydro-Quebec and the CCHRP team that were inside the study zones were utilized to validate the classified imagery.

### **3.3.8. Comparison To Aerial Photos**

To examine how our classified images perform at smaller scales, a subset of the aerial photos taken by Hydro-Quebec that were used to derive the eelgrass distribution maps was compared visually with our classified image at specific locations of the map in Figure 3.3. Each photograph was annotated with the limit of continuous and discontinuous eelgrass distribution for each site. These annotated aerial photographs correspond to field surveys from 1986 and 1995, so the classifications from 1988 and 1996 were compared to these photographs. This comparison was used to examine how closely our image classifications match the

ground-truth data at more fine resolutions than a bay-wide scale, as well as to assess the accuracy of our image classifications.

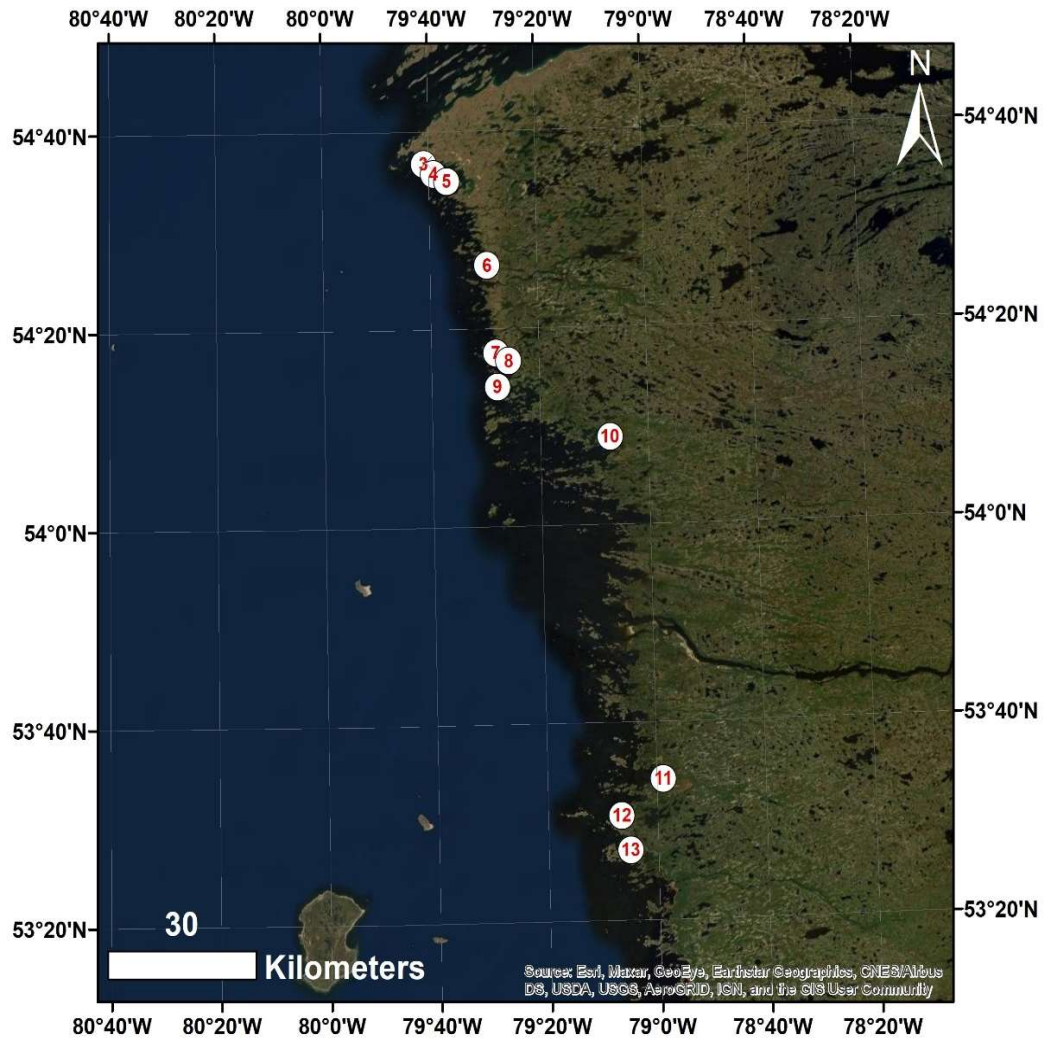


**Figure 3.3.** Locations of sites where aerial photographs with delineations of eelgrass extent were published

## 3.4. RESULTS

### 3.4.1. Image Classification and Validation

Spectral separability between classes varied widely between years, with an average of 1.982 (Table 3.5) (with 2 representing a perfect measure of class separability and 0 representing a complete lack of class separability). Separability between eelgrass and bare seafloor was the highest, averaging 1.992 across the four classification years. Low turbidity and deep water were the class pair with the lowest average separability (1.946) when averaging over the four years and had the lowest separability between class pairs in three of the four years. In comparison to the average separability across the years, the 1996 and 2019 Landsat images showed the highest average class spectral separability between all spectral class pairs. These two years also showed excellent separability between the eelgrass classes and all other class pairs, with average separability between eelgrass and all other classes of 1.996 and 1.999 for 1996 and 2019, respectively. The 1988 classification showed the worst average separation between eelgrass and the other class pairs evaluated, consistent with this year having the lowest overall separability between all the evaluated training class pairs.

The overall accuracies of each respective image classification displayed in Figure 3.4 were between 94.51% for the 1996 classification and 99.85% for the

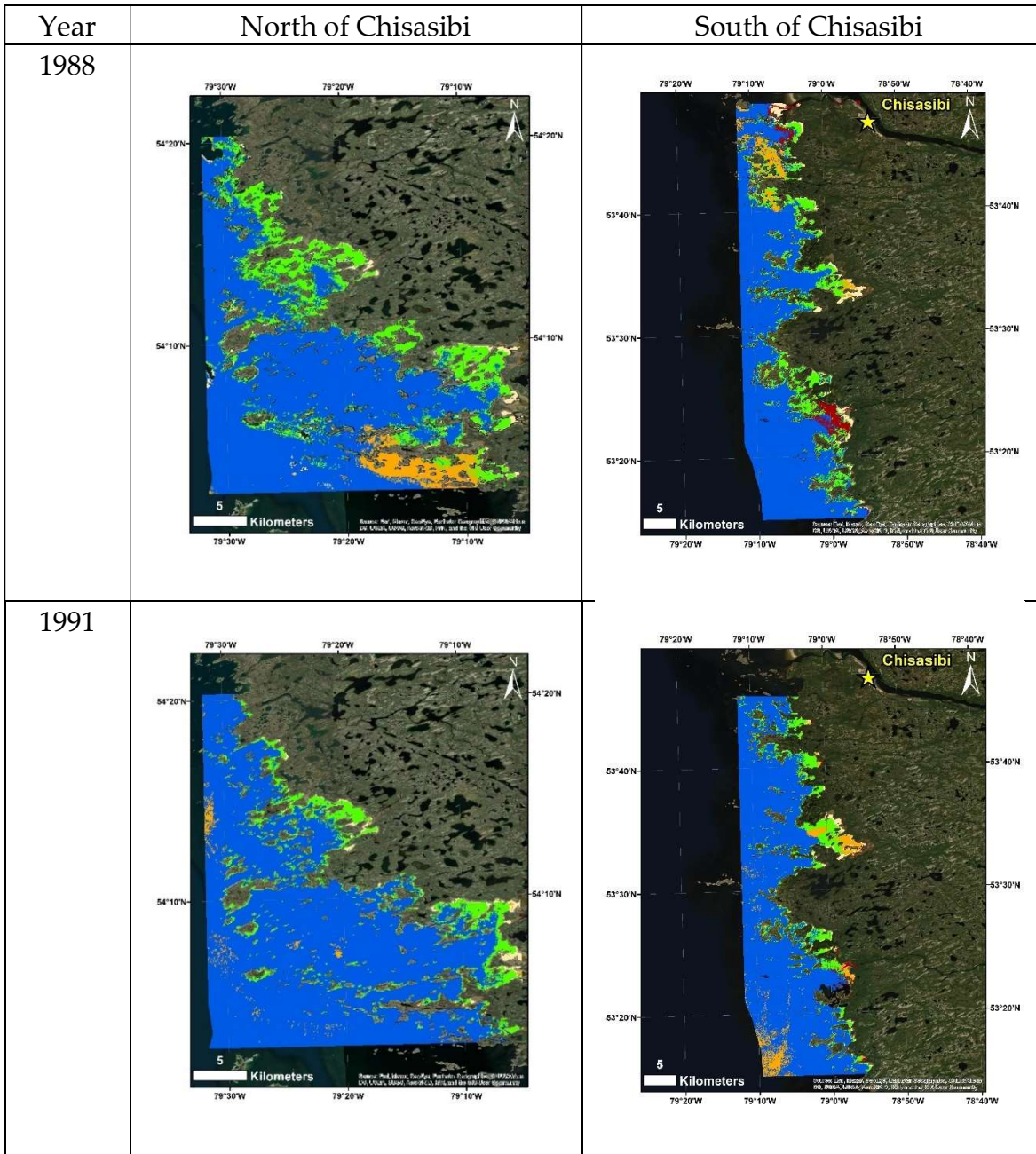
2019 classification (Table 3.6). Producer's accuracies for the "eelgrass" class were the lowest for the 1996 classification (89.29%) and the highest for the 2019 classification (99.95%). By all three metrics stated, the 2019 classification using Landsat-8 imagery was the most accurate of the four classified images, and the 1996 classification (LS5) was the least accurate.



**Table 3.6.** Confusion matrices showing classification accuracy evaluated with the OOB training areas for each classification year, expressed as a percentage of the total number of OOB training points for each year.

1988	Eelgrass	Low Turbidity	High Turbidity	Seafloor	Deep Water	Total	UA (%)
Eelgrass	<b>2.996</b>	0.029	0.011	0.025	0.256	3.318	90.32
Low Turbidity	0.049	<b>6.541</b>	0.007	0.017	0.059	6.673	98.02
High Turbidity	0.010	0.006	<b>1.345</b>	0.001	0.050	1.411	95.28
Seafloor	0.026	0.011	0.002	<b>1.895</b>	0.003	1.937	97.83
Deep Water	0.173	0.018	0.019	0.001	<b>86.449</b>	86.661	99.76
Total	3.255	6.604	1.384	1.940	86.817	<b>Total Points = 138230</b> <b>Overall Accuracy (%) = 99.23%</b>	
PA (%)	92.06	99.04	97.18	97.69	99.58		
1991	Eelgrass	Low Turbidity	High Turbidity	Seafloor	Deep Water	Total	UA (%)
Eelgrass	<b>2.910</b>	0.015	0.010	0.019	0.104	3.059	95.15
Low Turbidity	0.027	<b>37.390</b>	0.003	0.023	1.445	38.888	96.15
High Turbidity	0.014	0.005	<b>0.365</b>	0.002	0.035	0.421	86.57
Seafloor	0.015	0.045	0.000	<b>0.984</b>	0.000	1.044	94.2
Deep Water	0.026	1.348	0.010	0.000	<b>55.202</b>	56.587	97.55
Total	2.993	38.804	0.388	1.028	56.787	<b>Total Points = 99001</b> <b>Overall Accuracy (%) = 96.85</b>	
PA (%)	97.23	96.36	94.01	95.68	97.21		
1996	Eelgrass	Low Turbidity	High Turbidity	Seafloor	Deep Water	Total	UA (%)
Eelgrass	<b>3.239</b>	0.000	0.131	0.056	0.433	3.859	83.94
Low Turbidity	0.000	<b>11.776</b>	0.000	0.000	2.235	14.011	84.05
High Turbidity	0.140	0.005	<b>3.257</b>	0.043	0.154	3.599	90.48
Seafloor	0.068	0.000	0.030	<b>1.562</b>	0.000	1.661	94.09
Deep Water	0.180	1.954	0.063	0.000	<b>74.674</b>	76.871	97.14
Total	3.628	13.735	3.480	1.662	77.496	<b>Total points = 103941</b> <b>Overall Accuracy (%) = 94.51</b>	
PA (%)	89.29	85.74	93.59	94.04	96.36		

2019	Eelgrass	Low Turbidity	High Turbidity	Seafloor	Deep Water	Total	UA (%)
Eelgrass	<b>2.731</b>	0.000	0.000	0.000	0.005	2.736	99.8
Low Turbidity	0.000	<b>6.570</b>	0.000	0.000	0.038	6.608	99.43
High Turbidity	0.000	0.000	<b>2.047</b>	0.000	0.063	2.111	96.97
Seafloor	0.000	0.000	0.000	<b>0.765</b>	0.000	0.765	100
Deep Water	0.001	0.037	0.001	0.000	<b>87.741</b>	87.779	99.96
Total	2.732	6.608	2.048	0.766	87.846	<b>Total Points = 472643</b> <b>Overall Accuracy (%)</b> <b>= 99.85</b>	
PA (%)	99.95	99.44	99.96	99.97	99.88		



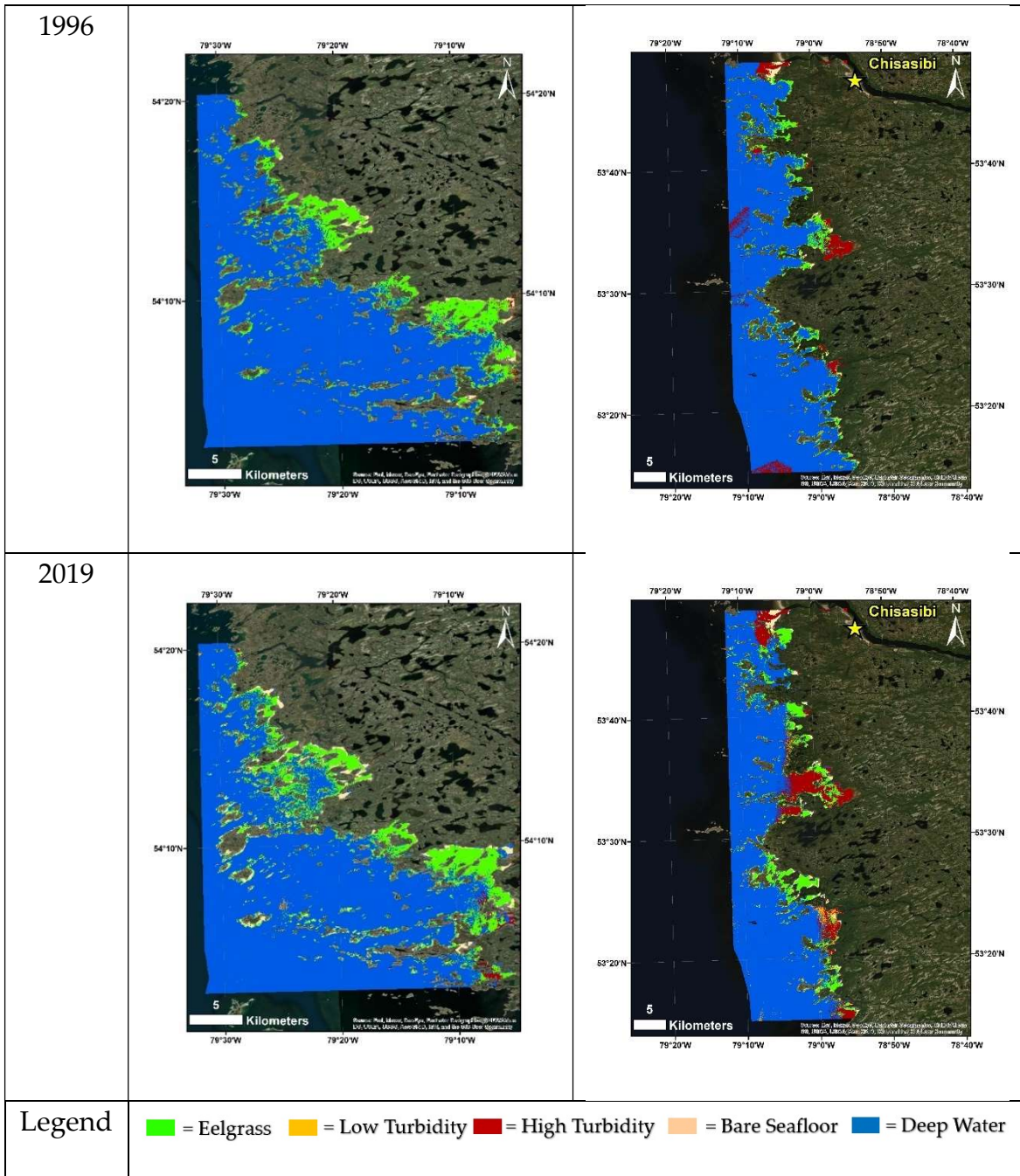


**Figure 3.4.** Classified images produced by applying the Random Forests classifier to all the reflectance images, associated vegetation indices, and bathymetric ratios for each year

To assess the importance of each inputted feature in the classification, we used the mean decrease in permutation accuracy statistic provided by Random Forest. Each variable was ranked relative to the other variables for each classification year and tabulated (Table 3.7). This analysis suggests that variable importance is not consistent across classification years, as well as between the two different optical sensors (Landsat-5 and Landsat-8) within the random forests classifier. The Green band reflectance was important in every classification (particularly for the 1991 classification), but the most important single band reflectance was from the coastal band in the 2019 classification. The Turbidity layer was very important for the 2019 classification. The relative depth variables were the two most important variables for 1988 and 1996. However, they were less important in 1991 (with RD2 ranking as the least important variable) and 2019. The SWIR2 layer was one of the least important variables across years, except for 1988. The vegetation indices were generally less important than the simple band reflectance or the bathymetric ratios.

**Table 3.7.** Importance of each input variable for increasing model accuracy ranked from the most (1) to the least important (24) as a function of the classification year.

<b>Model Importance Rank</b>	<b>1988</b>	<b>1991</b>	<b>1996</b>	<b>2019</b>
1	RDI2	Green	RDI1	Turbidity
2	RDI1	Blue	RDI2	SWIR1
3	Green	GDVI	GDVI	Coastal
4	SWIR2	NIR	Green	Blue
5	NIR	Blue/Red	NIR	GDVI
6	WAVI	RDI1	Red	Green
7	Turbidity	NG	Blue/Red	Blue/Green
8	Red	Blue/Green	DVI	WAVI
9	GDVI	Turbidity	Blue/Green	RDI1
10	Blue/Green	Red	Turbidity	Coastal/Green
11	Blue	WAVI	NDAVI	NIR
12	Blue/Red	DVI	RVI	NDAVI
13	DVI	NR	GNDVI	Red
14	NR	NDAVI	NG	NNIR
15	NDAVI	GRVI	NDVI	GRVI
16	NG	GNDVI	GRVI	GNDVI
17	RVI	NNIR	WAVI	RDI2
18	SWIR1	SWIR1	Blue	NDVI
19	NDVI	RVI	NNIR	RVI
20	GNDVI	NDVI	NR	SWIR2
21	GRVI	SWIR2	SWIR1	RDI2
22	NNIR	RDI2	SWIR2	GNDVI
23				RVI
24				SWIR2

Classified images were further assessed for accuracy using validation points (present/absent) derived from historical HQ eelgrass distribution maps for 1988, 1991, and 1996 as well as the JCCAP team’s field validation set for the 2019 classification and displayed as a confusion matrix for each classified image

(Table 3.8). The overall validation accuracy was the highest for the 1988 classification (84.5%) and the lowest for the 2019 classification (74.5%). Producer's accuracies of the eelgrass present class ranged from 73.3% with the 1996 classification to 84.00% with the 1988 classification, while the corresponding User's accuracies ranged from 79.2% with the 1988 classification to 91.1% with the 2019 classification, indicating reasonable consistency between classification results. The 1988 classification and the 2019 classification had significantly fewer validation points compared to the 1991 and 1996 classifications due to lack of data availability in 1988 and 2019. Yet, the results of the field validation do not show any distinct trends relative to the number of validation points.

**Table 3.8.** Confusion matrices showing classification accuracy evaluated with the ground-truth dataset for each classification year, expressed as a percentage of the total points used for each year.

		Ground-Truth				
1988	Class	Eelgrass Present	Eelgrass Absent	Total	UA (%)	EC (%)
Classified	Eelgrass Present	<b>34.15</b>	8.94	43.09	79.25	20.75
	Eelgrass Absent	6.50	<b>50.41</b>	56.91	88.57	11.43
	Total	40.65	59.35			
	PA (%)	84.00	84.93	Total Points = 123 Overall Accuracy (%) = 84.55		
	EO (%)	16.00	15.07			
		Ground-Truth				
1991	Class	Eelgrass Present	Eelgrass Absent	Total	UA (%)	EC (%)
Classified	Eelgrass Present	<b>37.50</b>	8.00	45.50	82.42	17.58
	Eelgrass Absent	12.50	<b>42.00</b>	54.50	77.06	22.94
	Total	50.00	50.00			
	PA (%)	75.00	84.00	Total Points = 200 Overall Accuracy (%) = 79.50		
	EO (%)	25.00	16.00			
		Ground-Truth				
1996	Class	Eelgrass Present	Eelgrass Absent	Total	UA (%)	EC (%)
Classified	Eelgrass Present	<b>36.67</b>	6.67	43.33	84.62	15.38
	Eelgrass Absent	13.33	<b>43.33</b>	56.67	76.47	23.53
	Total	50.00	50.00			
	PA (%)	73.33	86.67	Total Points = 180 Overall Accuracy (%) = 80.00		
	EO (%)	26.67	13.33			
		Ground-Truth				
2019	Class	Eelgrass Present	Eelgrass Absent	Total	UA (%)	EC (%)
Classified	Eelgrass Present	<b>69.49</b>	6.78	76.27	91.11	8.89
	Eelgrass Absent	18.64	<b>5.08</b>	23.73	21.43	78.57
	Total	88.14	11.86			
	PA (%)	78.85	42.86	Total Points = 59 Overall Accuracy (%) = 74.58		
	EO (%)	21.15	57.14			

(\*) *Bold figures indicated well-classified pixels; EC = Error of commission; EO = Error of omission; PA = Producer's accuracy; UA = User's accuracy.*

When the classified eelgrass area across each zone was quantified, a declining trend in eelgrass extent was observed throughout the study period for both zones as well as the total study period, although the 2019 extent was slightly higher than the 1991 and 1996 extents (Figure 3.5). Total eelgrass classified was not evaluated between 1996 and 2019 due to the absence of historical distribution data, therefore information during this specific period is lacking.

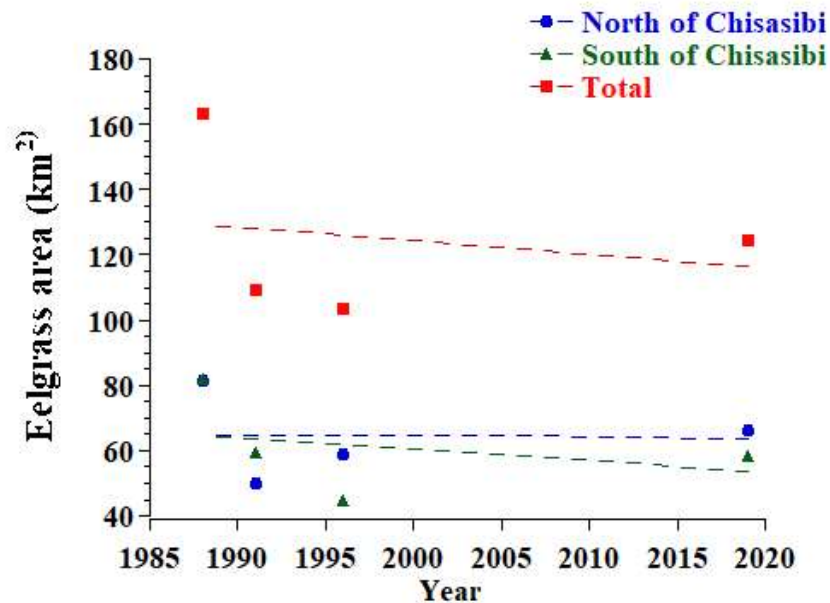


**Figure 3.5.** Evolution of the eelgrass area extracted from the classified imagery as a function of the classification year. The dotted lines represent trends over the course of the study period since no data exists between 1996 and 2019.

Due to variable extents of turbid water in each classification year, the total area having potentially eelgrass beds varies between the four classified images. To determine if this impacted the overall trend, the total area classified as eelgrass was also determined where all pixels classified as turbid water during any of the four image classifications were removed from all the classified images. This

allowed us to determine the total eelgrass area independent of the quantity of turbid water pixels present for each individual classification year. Table 3.9 gives the resulting eelgrass area with and without the turbid water pixels. The difference between the two cases is the largest for 1991 and 1996, indicating that the influence of water turbidity extent is the most important for both years.

**Table 3.9.** Total classified eelgrass area, assessed with turbid water points from any classified image omitted from all other images, as well as with turbid water points included.

	Turbid Pixels Included			Turbid Pixels Excluded		
	North	South	<u>Total</u>	<u>North</u>	<u>South</u>	<u>Total</u>
<u>1988</u>	82.39	86.89	169.28	79.39	62.82	142.21
<u>1991</u>	50.47	59.35	109.82	23.58	25.87	49.45
<u>1996</u>	60.00	45.51	105.51	30.24	14.81	45.05
<u>2019</u>	66.37	59.31	125.68	47.95	44.06	92.01

### 3.4.2. Eelgrass Distribution and Temporal Trends

Eelgrass was observed along most of the extent of the coast in the two zones evaluated (North of Chisasibi and South of Chisasibi). For both zones, there was a slight decrease in total classified eelgrass over the study period. However, the trend exhibited does not take into account changes in eelgrass distribution over the 22-year period from 1996 to 2019, since no historical distribution data was published for these years. To the North of Chisasibi, certain bays, such as the Bay of Many Islands (approximately 53° 8' N Latitude), appear to consistently hold large eelgrass meadows through all four classification years.

South of Chisasibi, large-scale trends are less apparent, partially due to the widespread classification of turbid water in the region. Dead Duck Bay, a large bay at around 53° 35' N Latitude, shows turbid water classified during all four

classification years. While eelgrass was still classified in the region, the comparison between our classifications and the HQ aerial photos in 1988 and 1996 suggested that this area was classified slightly less accurately than areas with less turbid water, indicating that turbid water likely decreases mapping accuracy in the zone south of Chisasibi. Total eelgrass extent extracted from the 1996 classified imagery appears to be substantially lower than the other classification years, especially towards the seaward extent of meadows, which may be indicative of higher tidal levels obfuscating eelgrass in deeper water.

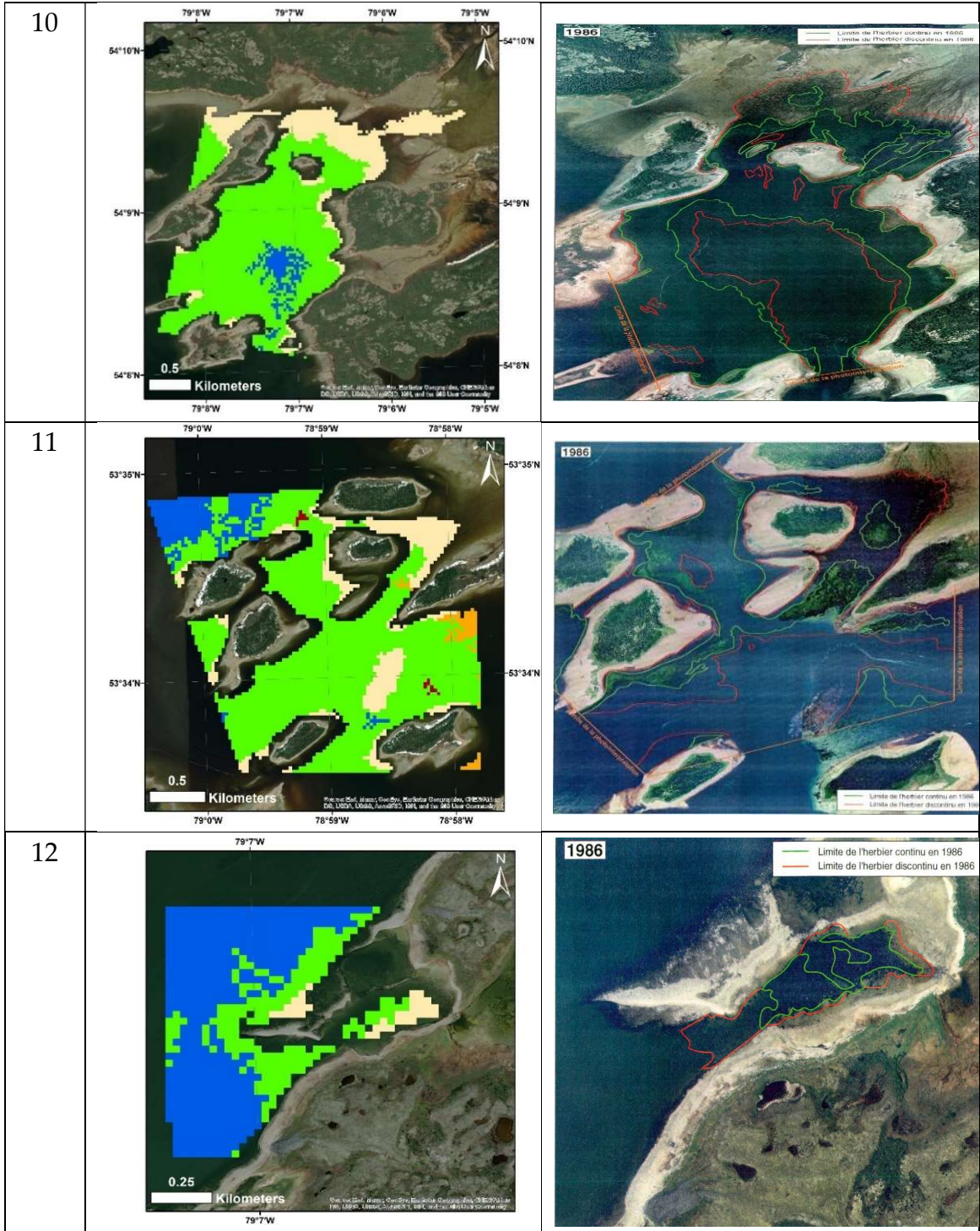
#### **3.4.3. Comparison to Historical Aerial Photos**

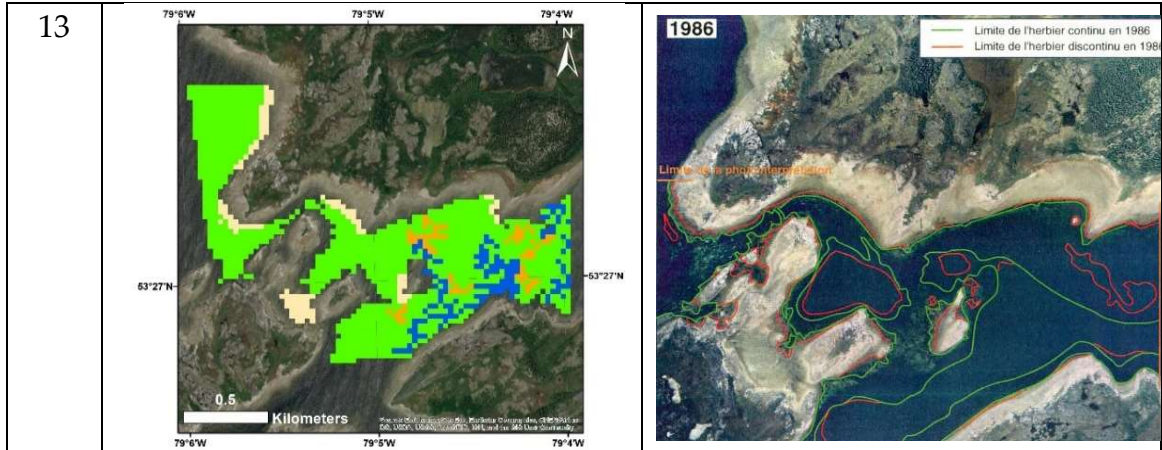
Since the aerial photograph delineations were not available for 1991, only the 1988 and 1996 classifications were compared at individual sites to aerial photographs with delineations of eelgrass distribution produced by HQ. Both data sources (classified imagery and historical aerial photographs) showed a general agreement that eelgrass was present along the entire eastern coastline of James Bay based on a visual comparison of the two images for each study site. Both datasets showed large eelgrass beds in locations where they have been historically recorded to be present, such as the Bay of Many Islands and Dead Duck Bay. A slight variation was observed between the three years on either the historical distribution maps or the multispectral image classifications between

the presence and general distribution of the most major beds, while higher variation was shown for smaller beds on the classified Landsat imagery.

Out of the seven sites analyzed in 1986, our classified imagery from 1988 closely resembles the outlined shape of the eelgrass meadows in five images (Figure 3.6). Generally, the edges of the eelgrass meadows did not perfectly match, but where eelgrass was delineated, it was always classified as eelgrass in the 1988 image classification. However, the 1988 image classification showed a slightly different eelgrass distribution than the aerial photos of 1986 since eelgrass is frequently classified just outside the aerial photo limits. The distribution and shape of eelgrass meadows, as extracted from the classified image of 1996, are generally in good agreement with those extracted from the aerial photographs of 1995. Out of 11 analyzed sites, the 1996 image classification closely resembles the outlined shape of the eelgrass meadow in ten aerial photographs. In the remaining image, eelgrass appears to be overestimated (Site 10), like many of the sites from 1988. In all sites where any pixels within the image bounds were classified as turbid water, eelgrass extent appeared to be overestimated by the classifier.

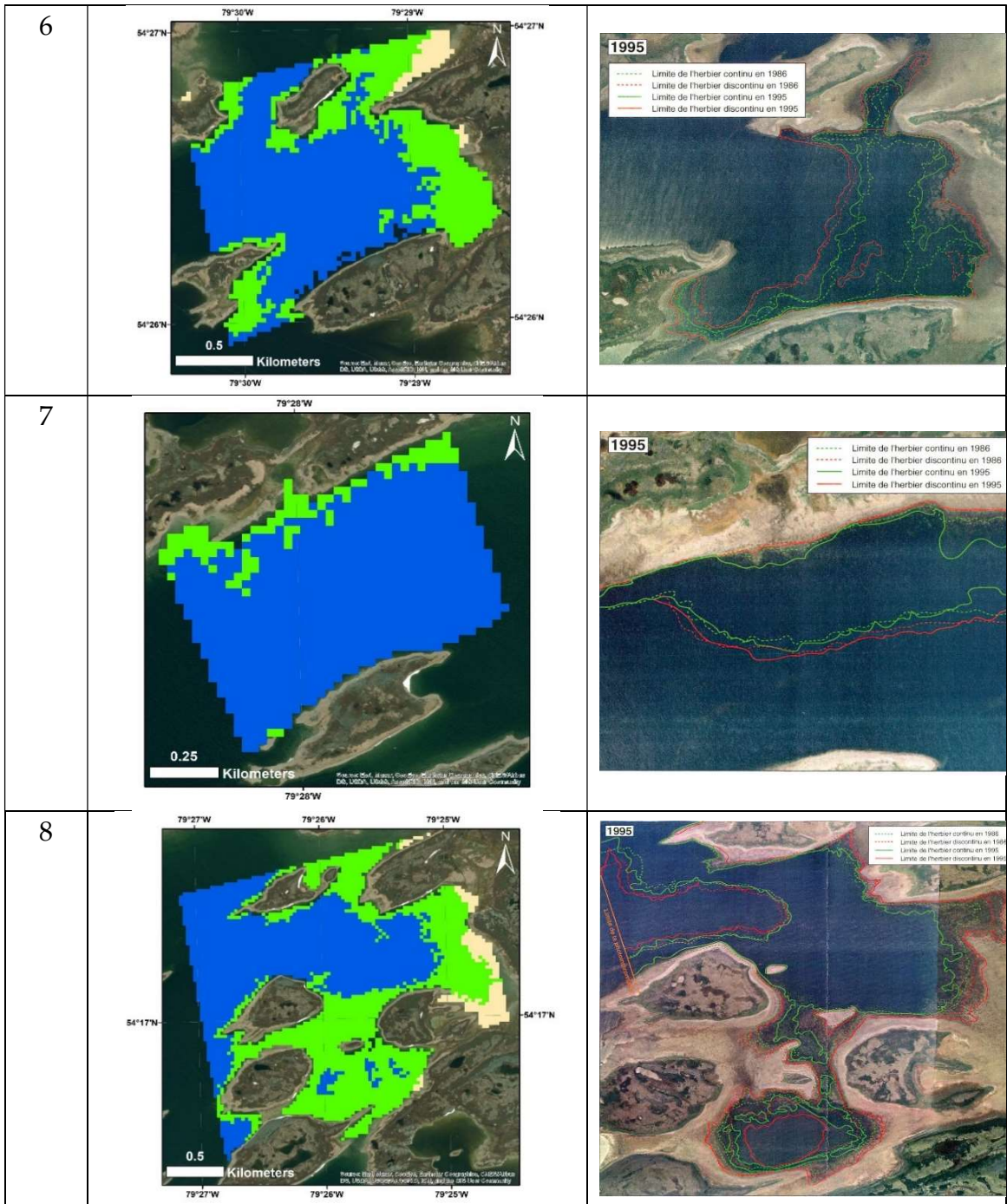
Site #	Classified Landsat Imagery (1988)	Aerial Photograph (1986)
7		
8		
9		

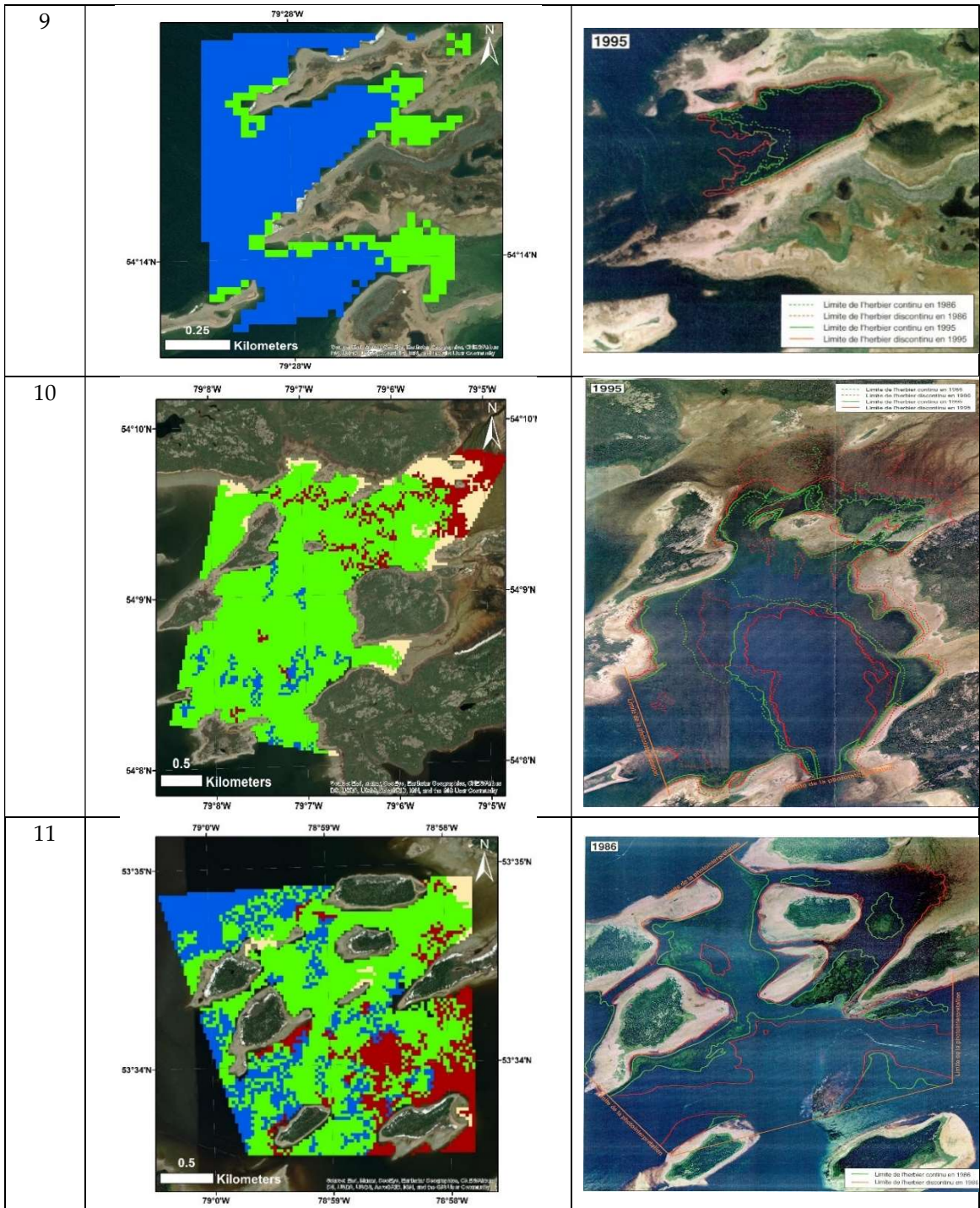




**Figure 3.6.** Comparison between the classified Landsat imagery of 1988 and the aerial photographs of 1986 for the limits of eelgrass distribution at sites 7-13. Green lines on the aerial photos represent the extent of continuous eelgrass beds, while the red lines represent the discontinuous bed extent.

Site #	Classified Landsat Imagery (1996)	Aerial Photograph (1995)
3		
4		
5		





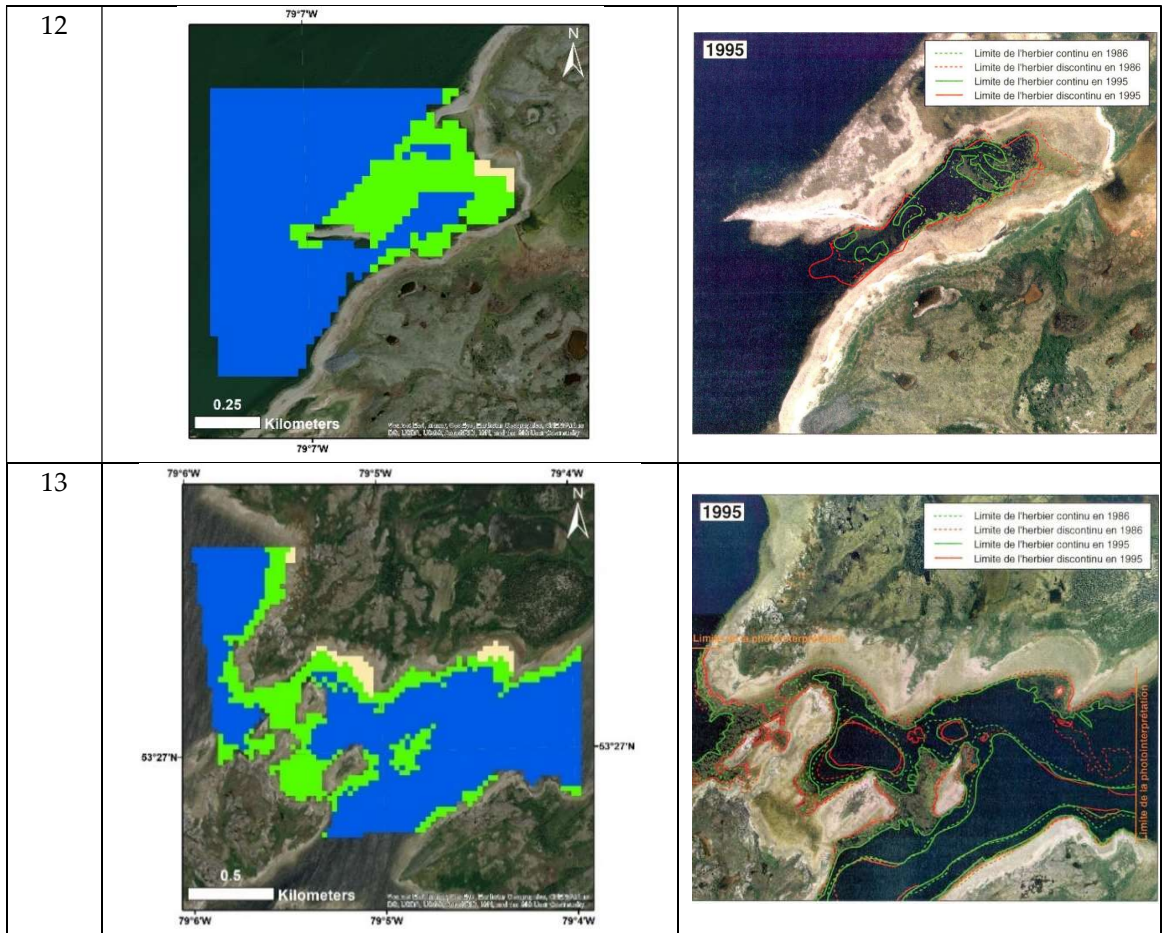


**Figure 3.7.** Comparison between the classified Landsat imagery of 1996 and the aerial photographs of 1995 for the eelgrass distribution. Green lines on the aerial photos represent the extent of continuous eelgrass beds, while the red lines represent the discontinuous bed limit.

## 3.5. DISCUSSION

### 3.5.1. Overall Mapping Accuracy

Satellite image analysis offers users the unique ability to evaluate data retroactively and in real-time, which can be a precious tool for scientists looking to add depth and consistency to temporal change analysis [51,52]. The overall accuracy of our classified Landsat imagery assessed using the training data subset ranged from 94% (lowest) for the 1996 classification to 99% (highest) for the 2019 classification, indicating exceptionally high accuracy. When evaluated using our independent field data sets, classified image accuracies for eelgrass presence/absence ranged between 74.6% for the 2019 classification (lowest) and 84.6% for the 1988 classification (highest), which, while lower, is still very accurate for the classification of multispectral imagery. Our results present better overall accuracies than previous studies carried out over the eastern coast of James Bay. In one, an unsupervised classifier was applied to Worldview-2 and RapidEye images [28], and another utilized a maximum likelihood classifier to PlanetScope images [22,23]. These earlier studies achieved overall accuracies of 72.7% and 73.7%, respectively, and used more expensive high-resolution imagery. Our overall mapping accuracies were greater than those of Traganos et al. (2018) (72%), who mapped the presence/absence of eelgrass beds in Greece using a Support Vector Machine through the Google Earth Engine system [53].

They were comparable and, in some instances, better than those using Sentinel-2 imagery for mapping eelgrass along Canada's Atlantic coast, such as Gallant et al. (2021) (79.00% and 72.58%) with random forests and Wilson et al. (2020) (78.72%) with a hierarchical classifier [54,55], showing that our approach utilizing supervised classification via random forests provides similar or better levels of accuracy to comparable studies in both James Bay and around the world.

### **3.5.2. Variable Importance in Random Forests**

Relative variable importance, as calculated in the Random Forests classifier, showed a lack of homogeneity between classification years, meaning variables did not show clearly distinctive patterns as to which were the most valuable contributors to mapping accuracy. The Relative Depth variables created (RDI1 & RDI2) were the two most important variables for 1988 and 1996, but their relative importance was not consistent between classification years; they were only the 6<sup>th</sup> and 22<sup>nd</sup> most important variables for the 1991 classification, and the 9<sup>th</sup> and 18<sup>th</sup> for 2019. In each classification, our model appeared to regard certain variables as important where they were not in another classification, such as the SWIR2 variable being 4<sup>th</sup> most important in 1988 and no better than 21<sup>st</sup> most important for any other classification year. Generally, each image classification used different variables to create the model equation, and no

variable was considered “ineffective” across all four image classifications. This suggests that the random forests classifier is likely information limited and will perform better when given a higher quantity of unique input variables.

### **3.5.3. Comparison to HQ Aerial Photographs**

Only image classifications from 1988 and 1996 were compared to the aerial photograph delineations of eelgrass extent produced by HQ since these maps were only produced for the summers of 1986 and 1995. Our image classification from 1996 showed exceptionally strong agreement between the aerial photograph interpretations from 1995 in both the presence and extent/shape of eelgrass beds, while the classification from 1988 matched only the presence of eelgrass beds at each aerial photography site. The 1988 image generally overestimated the extent of eelgrass compared to the HQ aerial photos, especially at sites 7 (southern extent), 9 (western extent), and 11 (southern extent). In both sets of imagery (1988 and 1996), eelgrass was present in all areas identified, indicating that the classifier does a suitable job at detecting the presence of large beds at relatively smaller scales (images were at a relative scale of approximately 1:10,000). In the 1988 comparison, turbid water was classified at sites 7, 11, and 13, which were all sites where eelgrass was overestimated relative to the assessment performed by HQ. A similar trend was exhibited in the 1996 comparison, where sites 10 and 11 had classified turbid water and showed an

apparent overestimation of eelgrass extent within the image's bounds. In all, the similarities exhibited between our image classifications at the sites where aerial photograph delineations were published suggest that our satellite image classifications may offer comparable accuracy to the photo interpretation of historical aerial photographs for mapping the extent of large eelgrass beds along the coast.

#### **3.5.4. Causes of the Water Turbidity**

Table 3.8 shows that the effect of water turbidity extent over the eelgrass extent was the most important in 1991 and 1996. Besides the hydro-electric development occurring in the area, another factor that could explain the water turbidity is extensive wildfires. According to Figure 3.8, the maximum burned area occurred in 1989. As shown in Figure 3.9, a large portion of that burned area occurred on or around watersheds of major James Bay tributaries. A comparison of satellite images acquired before and after the 1989 fires on these major James Bay tributaries showed a distinctive higher water turbidity on the post-fire images than on the pre-fire images (Figure 3.10).

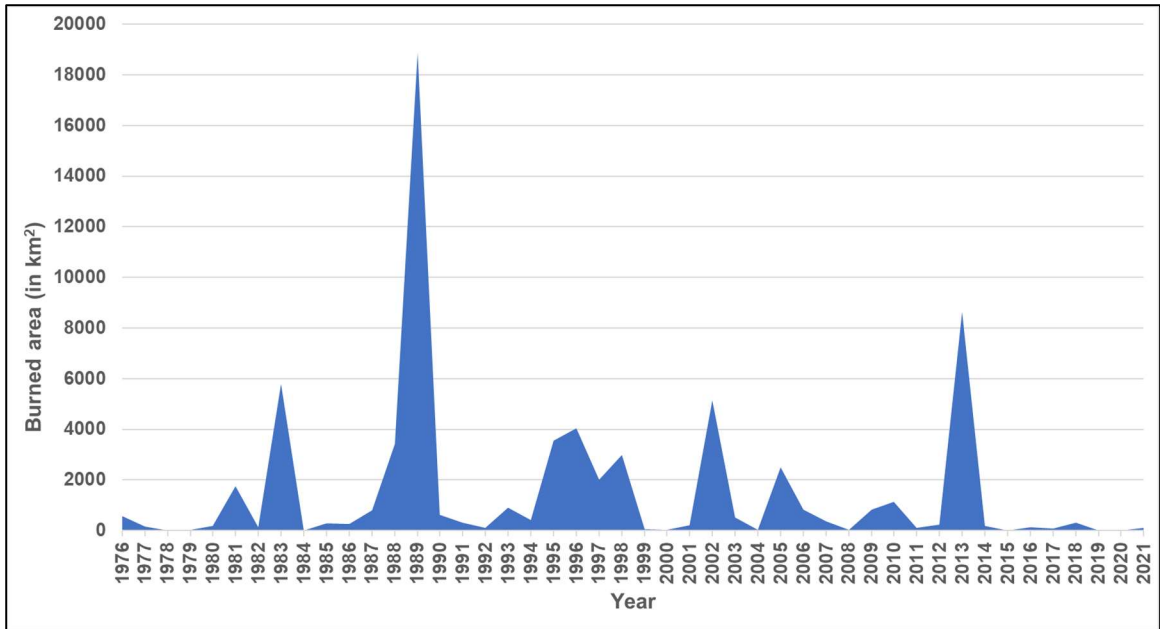


Figure 3.8. Evolution of the yearly burned areas extracted from the fire map of the Quebec Ministry of Forests, Wildlife and Parks website (<https://mffp.gouv.qc.ca/>)

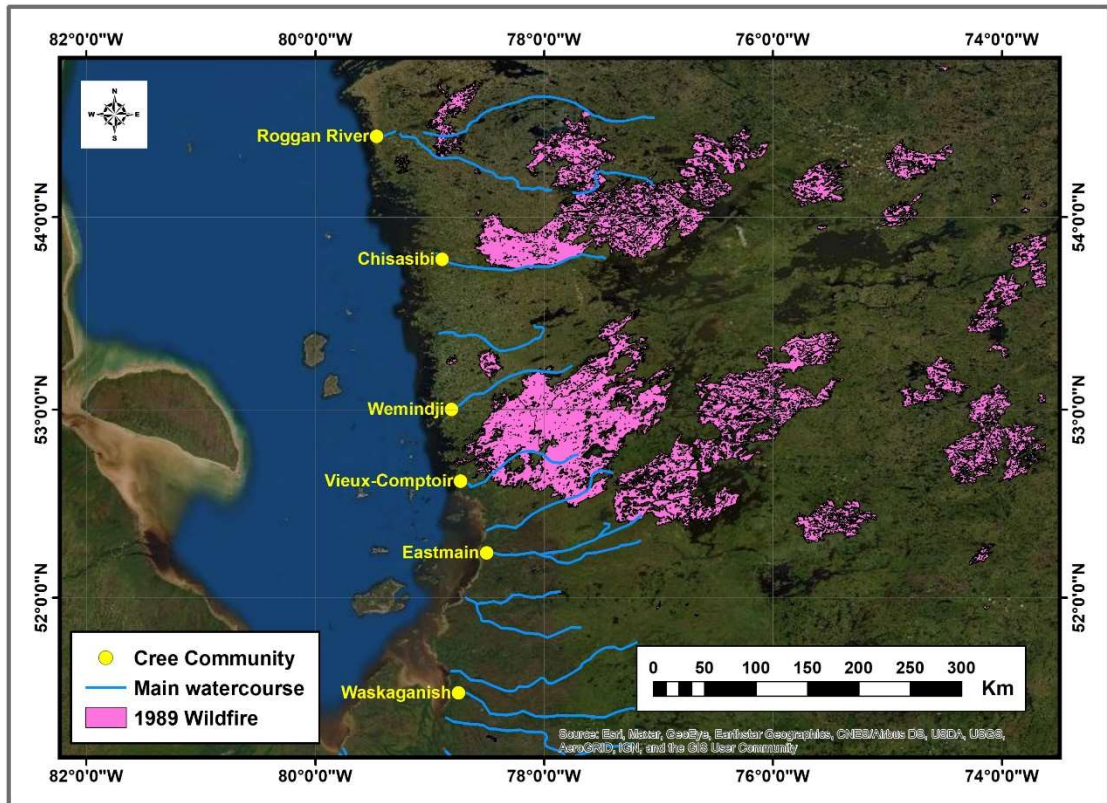












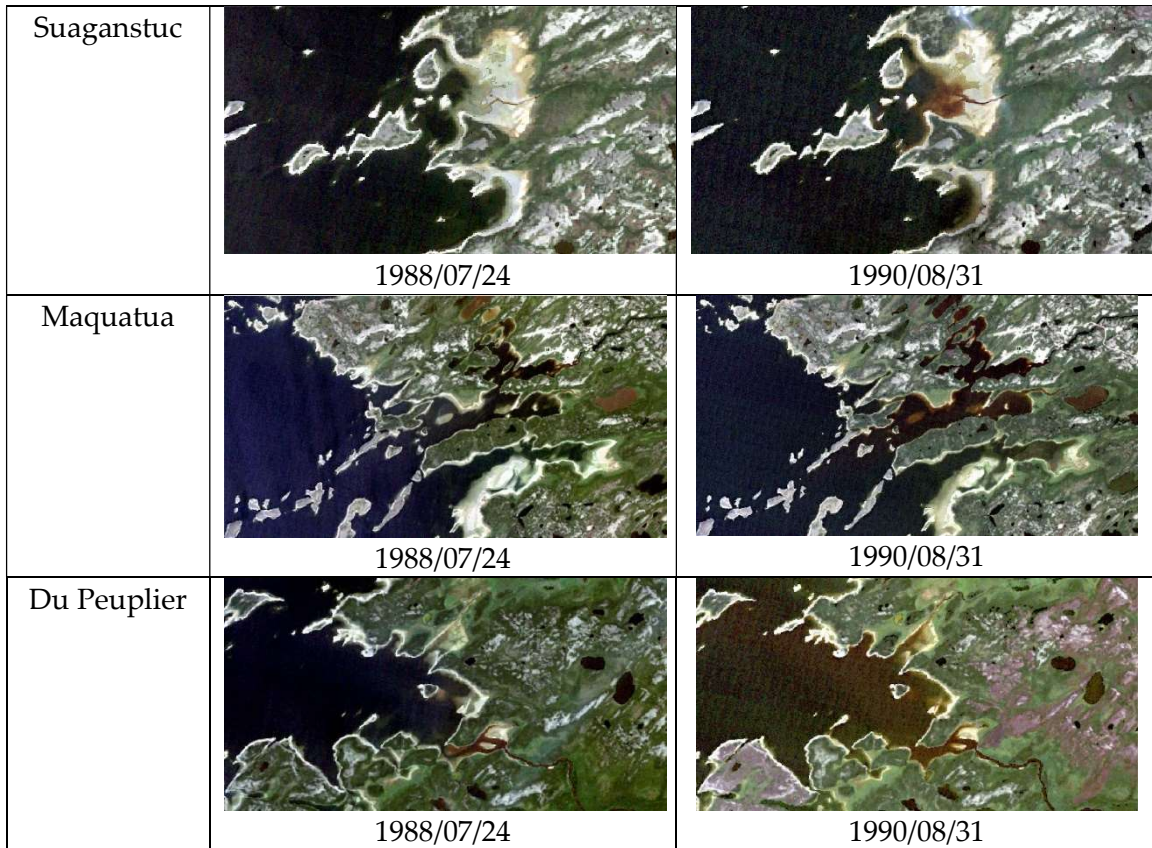


Figure 3.9. Distribution of the 1989 wildfires in Eeyou Istchee. Source: Quebec Ministry of Forests, Wildlife and Parks website (<https://mffp.gouv.qc.ca/>)

	Pre-fire	Post-fire
La Grande	 1988/07/24	 1989/09/13
Eastmain	 1988/07/24	 1989/09/23
Plagochioui	 1988/07/24	 1990/07/30
Morand	 1988/07/24	 1990/08/31
Guillaume	 1988/07/24	 1990/07/30
Castor	 1988/07/24	 1990/07/30



**Figure 3.10.** Comparison between Landsat RGB composites over major tributaries of the eastern coast of James Bay before and after the 1989 wildfires

### 3.5.5. Study Limitations

This study was limited by multiple factors, including: the availability of suitable ice and cloud-free imagery covering the whole of the study area and correct temporal period, tidal differences between images, limited spatial resolution and the quality of available ground-truth data. The imagery classified in this present study was acquired after the completion of most of the La Grande Complex, making it impossible to determine the potential effects of the hydroelectric project on eelgrass distribution in the bay. Even though historical data exists from before the complex's construction [14], there is no multispectral

satellite imagery from the Landsat collection to perform this analysis. In addition, some of the images acquired (i.e., 1988 and 1996) were acquired within two years of the data collected and published by Hydro-Quebec, limiting the precision with which we can compare our image classifications to preexisting historical data. Since cloud and ice-free imagery covering the full extent of the Eeyou Istchee coastline are scarce, tidal differences, which can affect the depth at which eelgrass can be detected, are reluctantly apparent between the three historical image classifications. Fortunately, Acolite automatically filters out “land pixels” (pixels where SWIR reflectance > 0) during atmospheric correction [30], so we can use a total number of pixels in each image as a proxy for tidal level. The tidal level, as measured by total water pixels, was lowest in the 1988 image and about 27% higher in 1991 (the image acquired at the highest tide). The tidal level was 11% higher (than in 1988) in both 1996 and almost exactly the same in 2019. This difference likely affects the extent to which eelgrass can be detected by the Landsat sensor, as eelgrass extent can be measured further out when the tidal level is lower, and there is less water column above the eelgrass to obfuscate the reflectance signal [56]. This discrepancy, therefore, presents a possible explanation as to why the extents of the classified eelgrass beds in the 1988 imagery were greater than the imagery in 1996 (Figures 3.6-3.7) and may have a substantial impact on the difference in total classified eelgrass detected in

the bay. However, in the absence of bathymetry data, it is impossible to estimate the exact effect of tidal differences in determining the total classified eelgrass area. In general, imagery acquired at the lowest possible tidal level should be prioritized when detecting submerged aquatic vegetation [57].

Landsat-derived image classifications, while effective for change detection in large areas, have many limitations on their applicability [58]. The moderate spatial resolution presents an advantage in covering a large aerial swath. However, mapping accuracy comes at a cost compared to utilizing imagery with higher spatial resolutions. [59–61]. Large eelgrass beds, mainly when a SIEVE filter was applied to the classified images, were easily detectable and their general shape and distribution were monitorable [50]. The SIEVE filter helped remove erroneously classified eelgrass pixels located in deep water. For a pixel to be classified as eelgrass, submerged aquatic vegetation should be the dominant reflectance signal in the area covered by the pixel (900 m<sup>2</sup>). Therefore, this approach cannot accurately reflect smaller eelgrass beds because of possible confusion with other features. Using this same logic, we can determine that our image classifications likely do not properly account for other vegetation types that are not eelgrass since there is only one class for SAV. While eelgrass is the dominant submerged vegetation across the eastern coast of James Bay, more localized populations of *Ruppia maritima*, *Ascophyllum nodosa*, or *Fucus vesiculosus*

could easily represent the dominant reflectance signal of a single pixel [5,17] and could also be misinterpreted as eelgrass when examining aerial photographs. While we can assume that eelgrass is most likely the only vegetation that would dominate the reflectance signal of multiple adjacent Landsat pixels in this region, this limitation outlines the need for diver-led field verification to assess the various types of submerged aquatic vegetation and their distribution within the study area [17,23].

### **3.6. CONCLUSIONS**

Our Landsat image classifications displayed the ability to map large eelgrass beds in James Bay with relatively strong accuracy on a large scale and accurately captured the presence and the extent of eelgrass beds at a relative scale of approximately 1:10,000 (dependent on the year and environmental factors including water turbidity and tidal level). Our classification accuracies, assessed using a subset of the training data and an independently generated ground-truth dataset, achieved comparable or better overall accuracies than other studies utilizing multispectral image classifications to map seagrasses in turbid, northern waters (including studies using higher resolution imagery) [22,62]. This study has also shown that our methodology is a reasonably cost-effective way to temporally monitor eelgrass beds in James Bay. The total costs associated with this mapping approach were kept low by utilizing publicly

available imagery and free, open-source atmospheric correction software, which limited the project's cost to the time required to perform and analyze the classified imagery and the fieldwork necessary to ground the truth of the data. Temporal trends exhibited in our study showed a decrease in the total extent of eelgrass classified over the studied period. The losses and gains for each zone evaluated can be attributed mainly to a few large eelgrass areas.

Since eelgrass growth and bed distribution can be limited mainly by light availability [63,64], depth can be a major factor in determining the location of eelgrass beds. Since no usable bathymetry data exists for James Bay, the addition of “relative depth” and “bathymetry ratios” were substituted to aid the classifier in ruling out eelgrass where the water depth was too low for growth (or too low to be accurately detected by the Landsat sensor). This study did not explore how the performance of these variables would compare to the addition of bathymetric data. However, adding bathymetric data to the classifier is recommended to enhance model accuracy. If available, other types of data (i.e., salinity, substrate type, acoustic sonar data, etc.) would likely also strengthen classification accuracy [56]. Another factor that can limit the availability of light for eelgrass is water turbidity, which makes it an important environmental parameter to monitor in James Bay. We showed that the 1989 wildfires had an effect on the river turbidity, but further research should be carried out to investigate more in

details the effects of wildfire on bay-wide turbidity, and further, how changes in water turbidity affect the health and distribution of eelgrass in James Bay.

Overall, in this study, we showed that multispectral image classification could be a valuable tool for detecting and mapping large eelgrass beds along the eastern coast of James Bay, even in locations with variably turbid water. Data from the Landsat archive is continuously collected and consistently updated within the USGS database, giving this type of study widespread applicability for both past and future change detection analysis. Multispectral image classification can be used on its own but is best used in conjunction with one or multiple field surveys or other datasets. Our classified image maps can and should be used to inform and guide future researchers on where eelgrass distribution might be changing or should be monitored along the eastern coastline of James Bay.

### 3.7. REFERENCES

1. Nienhuis, P.; Groenendijk, A. Consumption of Eelgrass (*Zostera marina*) by Birds and Invertebrates: An Annual Budget Available online: <https://www-jstor-org.proxy.hil.unb.ca/stable/24817532?Search=yes&resultItemClick=true&searchText=eelgrass&searchText=wave&searchText=action&searchUri=%2Faction%2FdoBasicSearch%3FQuery%3Deelgrass%2Bwave%2Baction%26amp%3Bacc%3Don%26amp%3Bwc%3Don%26amp%3Bfc> (accessed on 16 June 2020).
2. Kennedy, L.A.; Juanes, F.; El-Sabaawi, R. Eelgrass as Valuable Nearshore Foraging Habitat for Juvenile Pacific Salmon in the Early Marine Period. *Marine and Coastal Fisheries* **2018**, *10*, 190–203, doi:10.1002/mcf2.10018.

3. Wong, M.C.; Bravo, M.A.; Dowd, M. Ecological Dynamics of *Zostera marina* (Eelgrass) in Three Adjacent Bays in Atlantic Canada. *Botanica Marina* **2013**, *56*, 413–424, doi:10.1515/bot-2013-0068.
4. Lalumière, R.; Messier, D.; Fournier, J.J.; Peter McRoy, C. Eelgrass Meadows in a Low Arctic Environment, the Northeast Coast of James Bay, Québec. *Aquatic Botany* **1994**, *47*, 303–315, doi:10.1016/0304-3770(94)90060-4.
5. Dignard, N.; Lalumiere, R.; Reed, A.; Julien, M. *Habitats of the Northeast Coast of James Bay*; Environment Canada, Canada Wildlife Service, **1991**. 27p.
6. Kollars, N.M.; Henry, A.K.; Whalen, M.A.; Boyer, K.E.; Cusson, M.; Eklöf, J.S.; Hereu, C.M.; Jorgensen, P.; Kiriakopolos, S.L.; Reynolds, P.L.; et al. Meta-Analysis of Reciprocal Linkages between Temperate Seagrasses and Waterfowl with Implications for Conservation. *Frontiers in Plant Science* **2017**, *8*, 2119, doi:10.3389/fpls.2017.02119.
7. Olesen, B.; Krause-Jensen, D.; Marbà, N.; Christensen, P. Eelgrass *Zostera marina* in Subarctic Greenland: Dense Meadows with Slow Biomass Turnover in Cold Waters. *Marine Ecology Progress Series* **2015**, *518*, 107–121, doi:10.3354/meps11087.
8. Lalumière, R. *Étude de La Zostère Marine (Zostera marina) Sur La Côte Est de La Baie James - Été 1986*; **1986**. 112p.
9. Royer, M.-J.S. Eastern James Bay and the Cree. In *Climate, Environment and Cree Observations: James Bay Territory, Canada*; Royer, M.-J.S., Ed.; SpringerBriefs in Climate Studies; Springer International Publishing: Cham, **2016**; pp. 35–61 ISBN 978-3-319-25181-3.
10. Prevett, J.P.; Lumsden, H.G.; Johnson, F.C. Waterfowl Kill by Cree Hunters of the Hudson Bay Lowland, Ontario. *ARCTIC* **1983**, *36*, 185–192, doi:10.14430/arctic2261.
11. Rivers, D.O.; Short, F. Effect of Grazing by Canada Geese *Branta Canadensis* on an Intertidal Eelgrass *Zostera marina* Meadow. *Marine Ecology-progress Series - MAR ECOL-PROGR SER* **2007**, *333*, 271–279, doi:10.3354/meps333271.
12. COMEX Report on the Public Consultations Held in November 2012 Following Implementation of Hydro-Quebec's Eastmain-1-A and Sarcelle Powerhouses and Rupert Diversion Project **2013**. 238p.

13. COMEX *Eastmain-1-A and Sarcelle Powerhouses and Rupert Diversion. Followup of Eelgrass Beds on the Northeast Coast of Baie James (James Bay) - Study Report 2014.*; **2017**. 83p.
14. Curtis, S. Distribution of Eelgrass: East Coast, James Bay 1974. Map.
15. Lalumière, R. *Répartition De La Zostère Marine (Zostera marina) Sur La Côte Est De La Baie James - Été 1987*; Loretteville, Quebec, **1987**. **50p**.
16. Lalumiere, R.; Lemieux, C.; Belzile, L. *Répartition De La Zostere Maiune (Zostera marina L.) Sur La Côte Nord-Est De La Baie James - Été 1996*; **1996**;
17. Lalumiere, R. *Répartition De La Zostère Marine (Zostera marina) Sur La Côte Est De La Baie James - Été 1987*; **1987**. 50p.
18. Hydro-Quebec and GENIVAR Groupe Conseil Inc. *Environmental Monitoring of the La Grande Complex. Abridged Summary Report 1988-2000. Eelgrass Meadows of the Northeast Coast of James Bay.*; **2005**. 42p.
19. Leblanc, M.; O'Connor, M.; Kuzyk, Z.; Noisette, F.; David, K.; Richer, L.; Rabbitskin, E.; Sam, L.-L.; Gilbert, J.-P.; Leblon, B.; et al. *Large-Scale Regional Decline of Subarctic Zostera marina L. Eelgrass Followed by Differential Recovery Patterns along the Eastern Coast of James Bay, Canada: Insights from an Analysis of Long-Term Monitoring Data*; **2022**;
20. Kennedy, R.E.; Townsend, P.A.; Gross, J.E.; Cohen, W.B.; Bolstad, P.; Wang, Y.Q.; Adams, P. Remote Sensing Change Detection Tools for Natural Resource Managers: Understanding Concepts and Tradeoffs in the Design of Landscape Monitoring Projects. **2009**, doi:10.1016/j.rse.2008.07.018.
21. Stantec Consulting Ltd. Desktop Investigation of Eelgrass Along the Eastern Coast of James Bay. **2017**.
22. Stantec Consulting Ltd. *2017 Update: Desktop Investigation of Eelgrass Along the Eastern Coast of James Bay Using PlanetScope Imagery*; Dartmouth, Nova Scotia, **2019**. 37p.
23. Short, F.T.; Torio, D.; Anderson, N. James Bay Eelgrass Project - Final Report. **2019**. 85p.
24. Chavez, P.S. Image-Based Atmospheric Corrections - Revisited and Improved. *Photogrammetric Engineering & Remote Sensing* **1996**, 62, 1025–1036.

25. Aarts, L.; Larocque, A.; Leblon, B.; Douglas, A. Use of Uav Imagery for Eelgrass Mapping in Atlantic Canada. *ISPRS Annals of the Photogrammetry, Remote Sensing and Spatial Information Sciences* **2020**, *5*, 287–292, doi:10.5194/ISPRS-ANNALS-V-3-2020-287-2020.
26. Traganos, D.; Reinartz, P. Mapping Mediterranean Seagrasses with Sentinel-2 Imagery. *Marine Pollution Bulletin* **2018**, *134*, 197–209, doi:10.1016/J.MARPOLBUL.2017.06.075.
27. Fethers, J.O. Remote Sensing of Eelgrass Using Object-Based Image Analysis and Sentinel-2 Imagery. Master's Thesis. Aalborg University, Department of Geoinformatics. **2018**. 95p.
28. Keller, W.; Paterson, A.; Rühland, K.; Blais, J. Introduction — Environmental Change in the Hudson and James Bay Region. *Arctic, Antarctic, and Alpine Research* **2014**, *46*, 2–5, doi:10.1657/1938-4246-46.1.2.
29. O'Neill, J.D.; Costa, M.; Sharma, T. Remote Sensing of Shallow Coastal Benthic Substrates: In Situ Spectra and Mapping of Eelgrass (*Zostera marina*) in the Gulf Islands National Park Reserve of Canada. *Remote Sensing; Basel* **2011**, *3*, 975–1005, doi:http://dx.doi.org/10.3390/rs3050975.
30. Vanhellemont, Q. Adaptation of the Dark Spectrum Fitting Atmospheric Correction for Aquatic Applications of the Landsat and Sentinel-2 Archives. *Remote Sensing of Environment* **2019**, *225*, 175–192, doi:10.1016/j.rse.2019.03.010.
31. Vanhellemont, Q.; Ruddick, K. Atmospheric Correction of Metre-Scale Optical Satellite Data for Inland and Coastal Water Applications. *Remote Sensing of Environment* **2018**, *216*, 586–597, doi:10.1016/j.rse.2018.07.015.
32. Dogliotti, A.I.; Ruddick, K.G.; Nechad, B.; Doxaran, D.; Knaeps, E. A Single Algorithm to Retrieve Turbidity from Remotely-Sensed Data in All Coastal and Estuarine Waters. *Remote Sensing of Environment* **2015**, *156*, 157–168, doi:10.1016/j.rse.2014.09.020.
33. Mograne, M.; Jamet, C.; Loisel, H.; Vantrepotte, V.; Mériaux, X.; Cauvin, A. Evaluation of Five Atmospheric Correction Algorithms over French Optically-Complex Waters for the Sentinel-3A OLCI Ocean Color Sensor. *Remote Sensing* **2019**, *11*, 668, doi:10.3390/rs11060668.
34. De Keukelaere, L.; Sterckx, S.; Adriaensen, S.; Knaeps, E.; Reusen, I.; Giardino, C.; Bresciani, M.; Hunter, P.; Neil, C.; Van der Zande, D.; et al. Atmospheric

- Correction of Landsat-8/OLI and Sentinel-2/MSI Data Using ICOR Algorithm: Validation for Coastal and Inland Waters. *European Journal of Remote Sensing* **2018**, *51*, 525–542, doi:10.1080/22797254.2018.1457937.
35. Warren, M.A.; Simis, S.G.H.; Martinez-Vicente, V.; Poser, K.; Bresciani, M.; Alikas, K.; Spyarakos, E.; Giardino, C.; Ansper, A. Assessment of Atmospheric Correction Algorithms for the Sentinel-2A MultiSpectral Imager over Coastal and Inland Waters. *Remote Sensing of Environment* **2019**, *225*, 267–289, doi:10.1016/j.rse.2019.03.018.
  36. Vanhellemont, Q. Adaptation of the Dark Spectrum Fitting Atmospheric Correction for Aquatic Applications of the Landsat and Sentinel-2 Archives. *Remote Sensing of Environment* **2019**, *225*, 175–192, doi:10.1016/j.rse.2019.03.010.
  37. Vanhellemont, Q.; Ruddick, K. Advantages of High Quality SWIR Bands for Ocean Colour Processing: Examples from Landsat-8. *Remote Sensing of Environment* **2015**, *161*, 89–106, doi:10.1016/j.rse.2015.02.007.
  38. Forsey, D.; LaRocque, A.; Leblon, B.; Skinner, M.; Douglas, A. Refinements in Eelgrass Mapping at Tabusintac Bay (New Brunswick, Canada): A Comparison between Random Forest and the Maximum Likelihood Classifier. *Canadian Journal of Remote Sensing* **2020**, *46*, 640–659.
  39. Stumpf, R.P.; Holderied, K.; Sinclair, M. Determination of Water Depth with High-Resolution Satellite Imagery over Variable Bottom Types. *Limnology and Oceanography* **2003**, *48*, 547–556, doi:10.4319/lo.2003.48.1\_part\_2.0547.
  40. Tucker, C.J. Red and Photographic Infrared Linear Combinations for Monitoring Vegetation. *Remote Sensing of Environment* **1979**, *8*, 127–150, doi:10.1016/0034-4257(79)90013-0.
  41. Sripada, R.P.; Heiniger, R.W.; White, J.G.; Meijer, A.D. Aerial Color Infrared Photography for Determining Early In-Season Nitrogen Requirements in Corn. *Agronomy Journal* **2006**, *98*, 968–977, doi:10.2134/agronj2005.0200.
  42. Buschmann, C.; Nagel, E. In Vivo Spectroscopy and Internal Optics of Leaves as Basis for Remote Sensing of Vegetation. *International Journal of Remote Sensing* **1993**, *14*, 711–722, doi:10.1080/01431169308904370.
  43. Villa, P.; Mousivand, A.; Bresciani, M. Aquatic Vegetation Indices Assessment through Radiative Transfer Modeling and Linear Mixture Simulation.

- International Journal of Applied Earth Observation and Geoinformation* **2014**, *30*, 113–127, doi:10.1016/j.jag.2014.01.017.
44. Rouse, J.; Haas, R.H.; Schell, J.A.; Deering, D. Monitoring Vegetation Systems in the Great Plains with ERTS. *NASA. Goddard Space Flight Center 3d ERTS-1 Symp.* **1973**, *1*.
  45. Birth, G.S.; McVey, G.R. Measuring the Color of Growing Turf with a Reflectance Spectrophotometer <sup>1</sup>. *Agronomy Journal* **1968**, *60*, 640–643, doi:10.2134/agronj1968.00021962006000060016x.
  46. Horning, N. *Random Forests : An Algorithm for Image Classification and Generation of Continuous Fields Data Sets*; **2010**. 6p.
  47. El-Sabh, M.I.; Koutitonsky, V.G. An Oceanographic Study of James Bay before the Completion of the La Grande Hydroelectric Complex. *ARCTIC* **1977**, *30*, 169–186, doi:10.14430/arctic2697.
  48. Breiman, L. Random Forests. *Machine Learning* **2001**, *45*, 5–32, doi:10.1023/A:1010933404324.
  49. Waske, B.; Braun, M. Classifier Ensembles for Land Cover Mapping Using Multitemporal SAR Imagery. *ISPRS Journal of Photogrammetry and Remote Sensing* **2009**, *64*, 450–457, doi:10.1016/j.isprsjprs.2009.01.003.
  50. Sieve Classes Available online: <https://www.l3harrisgeospatial.com/docs/SievingClasses.html> (accessed on 24 June 2022).
  51. Wu, E.; Islam, K.; Li, J.; Lebrasse, M.C.; Hill, V.; Zimmerman, R. An Active Learning Model for Seagrass Detection in Remote Sensing Imagery. *2021 IEEE 12th Annual Information Technology, Electronics and Mobile Communication Conference, IEMCON 2021* **2021**, 113–118, doi:10.1109/IEMCON53756.2021.9623139.
  52. Ferguson, R.L.; Korfmacher, K. Remote Sensing and GIS Analysis of Seagrass Meadows in North Carolina, USA. *Aquatic Botany* **1997**, *58*, 241–258, doi:10.1016/S0304-3770(97)00038-7.
  53. Traganos, D.; Aggarwal, B.; Poursanidis, D.; Topouzelis, K.; Chrysoulakis, N.; Reinartz, P. Towards Global-Scale Seagrass Mapping and Monitoring Using

- Sentinel-2 on Google Earth Engine: The Case Study of the Aegean and Ionian Seas. *Remote Sensing* **2018**, *10*, doi:10.3390/RS10081227.
54. Gallant, E.; LaRocque, A.; Leblon, B.; Douglas, A. Eelgrass Mapping with Sentinel-2 and UAV Multispectral Imagery in Atlantic Canada. **2021**, 7939–7942, doi:10.1109/IGARSS47720.2021.9554760.
  55. Wilson, K.L.; Wong, M.C.; Devred, E. Branching Algorithm to Identify Bottom Habitat in the Optically Complex Coastal Waters of Atlantic Canada Using Sentinel-2 Satellite Imagery. *Frontiers in Environmental Science* **2020**, *8*, doi:10.3389/FENVS.2020.579856.
  56. Kuhwald, K.; Schneider von Deimling, J.; Schubert, P.; Oppelt, N. How Can Sentinel-2 Contribute to Seagrass Mapping in Shallow, Turbid Baltic Sea Waters? *Remote Sensing in Ecology and Conservation* **2021**, doi:10.1002/RSE2.246.
  57. Hoang, T.; Garcia, R.; O’Leary, M.; Fotedar, R. Identification and Mapping of Marine Submerged Aquatic Vegetation in Shallow Coastal Waters with WorldView-2 Satellite Data. *Journal of Coastal Research* **2016**, 1287–1291.
  58. Kovacs, E.; Roelfsema, C.; Lyons, M.; Zhao, S.; Phinn, S. Seagrass Habitat Mapping: How Do Landsat 8 OLI, Sentinel-2, ZY-3A, and Worldview-3 Perform? *Remote Sensing Letters* **2018**, *9*, 686–695, doi:10.1080/2150704X.2018.1468101.
  59. Topouzelis, K.; Makri, D.; Stoupas, N.; Papakonstantinou, A.; Katsanevakis, S. Seagrass Mapping in Greek Territorial Waters Using Landsat-8 Satellite Images. *International Journal of Applied Earth Observation and Geoinformation* **2018**, *67*, 98–113, doi:10.1016/j.jag.2017.12.013.
  60. O’Neill, J.D.; Costa, M. Mapping Eelgrass (*Zostera marina*) in the Gulf Islands National Park Reserve of Canada Using High Spatial Resolution Satellite and Airborne Imagery. *Remote Sensing of Environment* **2013**, *133*, 152–167, doi:10.1016/j.rse.2013.02.010.
  61. Pu, R.; Bell, S.; Meyer, C.; Baggett, L.; Zhao, Y. Mapping and Assessing Seagrass along the Western Coast of Florida Using Landsat TM and EO-1 ALI/Hyperion Imagery. *Estuarine, Coastal and Shelf Science* **2012**, *115*, 234–245, doi:10.1016/j.ecss.2012.09.006.
  62. Stantec Consulting Ltd. *Accuracy Assessment of Remote Sensing Methodologies for Tabusintac Bay, New Brunswick. Report for the Canadian Wildlife Service, Environment Canada, Sackville (NB).*; Dartmouth, Nova Scotia, **2016**. 42p.

63. Olesen, B.; Sand-Jensen, K. Patch Dynamics of Eelgrass *Zostera marina*. *Marine Ecology Progress Series* **1994**, *106*, 147–156, doi:10.3354/meps106147.
64. Jacobs, W.M., René, P.; Peter McRoy, C. Biomass Potential of Eelgrass (*Zostera marina* L.). *Critical Reviews in Plant Sciences* **1984**, *2*, 49–80, doi:10.1080/07352688409382188.

## CHAPTER 4: GENERAL DISCUSSION

The overall objective of this thesis was to evaluate the use of multispectral satellite imagery and supervised image classification with Random Forests to detect and map eelgrass along the eastern coast of James Bay, as well as to utilize our devised methodology to construct a time series of eelgrass distribution from 1988 – 2019. The thesis presented outlines a general methodology for acquiring and classifying multispectral satellite imagery, as well as validating the subsequent classified imagery using preexisting and independent historical eelgrass distribution data. Overall, multispectral satellite image classification was found to be an effective method of detecting the general shape and presence of large eelgrass meadows in James Bay, and our time-series of eelgrass distribution along the coast provides valuable insight into eelgrass distribution trends within the bay during this period, as well as a framework for future monitoring efforts.

The first objective of my thesis (Chapter 2) was to evaluate the capability of the Landsat-8 Operational Land Imager (OLI) sensor to detect and map eelgrass beds in James Bay and to create a baseline distribution map of eelgrass distribution in Eeyou Istchee for the year 2019. Our final classified image, when validated against a ground-truth dataset that consisted of 108 presence/absence points acquired in the summer of 2019, had an overall accuracy of 78.7%, which is equivalent to or higher than comparable studies utilizing a supervised

classification of multispectral imagery. Evaluated using a subset of the training data within the Random Forests classifier, our classified image produced an accuracy of 99.3%, indicating exceptionally high accuracy and the strong ability of the classifier to create separability between each of the respective classes.

Atmospheric correction of multispectral satellite imagery is necessary to obtain accurate information about environmental features [1,2]. For this study, Acolite was found to be a good option for atmospheric correction of the top-of-atmosphere (TOA) imagery coming from the U.S. Geological Survey (USGS) due mainly to its useability in turbid coastal waters [3,4]. The processes for atmospheric correction, sun glint correction, land and cloud masking, and image merging were all performed within the Acolite software, which offered a user-friendly approach to creating reflectance imagery for remote sensing analysis at zero cost [5]. Multiple input variables were also derived within the software and used as input variables for the Random Forests classifier. Class separability for the turbidity [6], suspended material [7] and orange band layers [8] overlapped significantly, indicating they may have provided the classifier with redundant information. The separability between classes was also relatively low for the floating algal index [9] and is likely not worth incorporating into future studies. Each of the vegetation indices and bathymetric ratios provided more class

separability and were likely important contributions to the model for increasing mapping accuracy.

Overall, eelgrass was detected in bands along the coast everywhere north of Eastmain during the summer of 2019. South of this point (and around the mouth of the Eastmain River), most of the water was classified as turbid, indicating that eelgrass cannot be detected there by our Landsat-8 OLI sensor and likely would have more trouble growing due to lack of light than eelgrass along the Northern section of the coast [10,11]. Eelgrass was not detected around Chisasibi and outside of the La Grande, consistent with reports from the Cree experience as well as Hydro-Quebec (HQ) [12,13], most likely caused by persistently low levels of salinity around this region [14,15]. Turbid water was classified abundantly around Wemindji and in many bays south of Chisasibi, where ground-truth data was collected, indicating these could be areas where the classifier may lack the ability to map the distribution of eelgrass accurately and consistently. Extra field verification work may be required.

The second objective of this thesis (Chapter 3) was to evaluate the use of images from the Landsat archive, including Landsat-5 Multispectral Instrument (MSI) and Landsat-8 OLI imagery, in conjunction with freely available historical data acquired by HQ, to map and monitor historical eelgrass distribution

changes in James Bay. We incorporated a similar methodology outlined in Chapter 2 (adjusted to fit the limitations of the Landsat-5 sensor), as well as eelgrass distribution maps produced by HQ through the interpretation of aerial photography in 1987, 1991, and 1996 to both train and validate our image classification models. Our historical classifications from 1988, 1991, and 1996 using Landsat-5 imagery yielded classification accuracies ranging from 79.5 – 84.5% when assessed for accuracy using a randomly generated validation data set, which is very accurate compared to similar studies and consistent between image classifications [16–18]. The image classification from 2019 using Landsat-8 imagery and the same input variables achieved an overall accuracy of 74.5%, assessed by the field validation set within the study area. Overall accuracies acquired using a subset of the training data ranged from 94.1 – 99.8%, indicating exceptionally strong mapping accuracies and strong model separability between training classes within the image.

Our historical image classifications were also analyzed by comparing the images to aerial photographs published by HQ, which are overlaid with the limit of eelgrass extent determined through photointerpretation of the aerial photography [19]. In this comparison, our classifications appeared to closely resemble the extents published by HQ in both the summers of 1987 and 1995. Our imagery acquired from 1988 seemed to show a greater seaward eelgrass

extent than the aerial photos from HQ, indicating either a potential error in the classification at identifying the boundaries of eelgrass meadows or possibly the sensor being able to detect eelgrass at deeper depths than aerial photograph interpreters. In the absence of in situ reflectance data as well as data on bathymetry, it is not easy to estimate the depth at which the Landsat-8 OLI sensor might be able to penetrate the water and detect eelgrass. In addition, varying levels of turbidity might make this value variable dependent on location along the coast [20].

Our classified historical imagery and a present-day map of eelgrass distribution from 2019 help add context to information about eelgrass distribution in the bay during this period. Eelgrass is present all along the coast in all three of our historical classification years, a trend that persists into 2019. Overall, the total eelgrass extent along the coast of Eeyou Istchee appears to have declined over the period, though this decline is more pronounced in certain areas, whereas others seem to be less affected during this period. Our historical reconstruction began with 1988 imagery, but the construction of the La Grande Complex occurred in the 1970s. Additional work is needed to compare our maps with older maps of the area.

Both papers (Chapters 2 and 3) presented in this thesis outline similar recommendations for future research. When utilizing supervised classification to map eelgrass beds in turbid, coastal waters, remote sensing specialists should coordinate as closely as possible with the field data acquisition team to get the most optimal data for ground-truthing and model training. Information on depth, bottom type, or even qualitative descriptions of eelgrass distribution trends within a confined area (i.e., eelgrass was not shown to grow past 10 m from the shoreline in this defined region) could aid the training area creation and thus the optimization of the classification model. In addition, higher resolution imagery would likely improve the potential of the classifier to detect eelgrass beds and improve the relative spatial scale at which their extent can be measured. While only Landsat was used for my study due to its historical applicability, a modern sensor with higher resolution (such as Sentinel-2 Multispectral Instrument) could allow for a more robust analysis. However, it may require more ground-truth data to accurately assess the results' quality. At which point, a field survey utilizing aerial photos or bottom-detecting sonar could provide a more practical option.

In conclusion, this study showed that eelgrass in James Bay could be detected and mapped by utilizing freely available multispectral imagery from the Landsat archive and open-source software packages for atmospheric

correction and image classification. Using historically collected (1987-1995) and modern field datasets (2019), we verified our classified image maps spanning approximately 40 years. These maps should aid researchers hoping to evaluate past and future changes to eelgrass distribution and dynamics along the Eeyou Istchee coastline. In addition, my study serves as a framework for any researcher aiming to utilize supervised classification of multispectral satellite imagery to detect eelgrass in northern coastal waters.

## REFERENCES

1. Kotchenova, S.Y.; Vermote, E.F.; Matarrese, R.; Klemm, F.J. Validation of a Vector Version of the 6S Radiative Transfer Code for Atmospheric Correction of Satellite Data. Part I: Path Radiance. *Applied Optics* **2006**, *45*, 6762–6774, doi:10.1364/AO.45.006762.
2. Warren, M.A.; Simis, S.G.H.; Martinez-Vicente, V.; Poser, K.; Bresciani, M.; Alikas, K.; Spyrakos, E.; Giardino, C.; Ansper, A. Assessment of Atmospheric Correction Algorithms for the Sentinel-2A MultiSpectral Imager over Coastal and Inland Waters. *Remote Sensing of Environment* **2019**, *225*, 267–289, doi: 10.1016/j.rse.2019.03.018.
3. Vanhellemont, Q.; Ruddick, K. Atmospheric Correction of Metre-Scale Optical Satellite Data for Inland and Coastal Water Applications. *Remote Sensing of Environment* **2018**, *216*, 586–597, doi: 10.1016/j.rse.2018.07.015.
4. Mograne, M.; Jamet, C.; Loisel, H.; Vantrepotte, V.; Mériaux, X.; Cauvin, A. Evaluation of Five Atmospheric Correction Algorithms over French Optically Complex Waters for the Sentinel-3A OLCI Ocean Color Sensor. *Remote Sensing* **2019**, *11*, 668, doi:10.3390/rs11060668.
5. Vanhellemont, Q. Adaptation of the Dark Spectrum Fitting Atmospheric Correction for Aquatic Applications of the Landsat and Sentinel-2 Archives. *Remote Sensing of Environment* **2019**, *225*, 175–192, doi: 10.1016/j.rse.2019.03.010.

6. Dogliotti, A.I.; Ruddick, K.G.; Nechad, B.; Doxaran, D.; Knaeps, E. A Single Algorithm to Retrieve Turbidity from Remotely Sensed Data in All Coastal and Estuarine Waters. *Remote Sensing of Environment* **2015**, *156*, 157–168, doi: 10.1016/j.rse.2014.09.020.
7. Nechad, B.; Ruddick, K.G.; Park, Y. Calibration and Validation of a Generic Multisensor Algorithm for Mapping of Total Suspended Matter in Turbid Waters. *Remote Sensing of Environment* **2010**, *114*, 854–866, doi: 10.1016/j.rse.2009.11.022.
8. Castagna, A.; Simis, S.; Dierssen, H.; Vanhellemont, Q.; Sabbe, K.; Vyverman, W. Extending Landsat 8: Retrieval of an Orange Contra-Band for Inland Water Quality Applications. *Remote Sensing* **2020**, *12*, 637, doi:10.3390/rs12040637.
9. Dogliotti, A.; GosGossen.; Vanhellemont, Q.; Ruddick, K. Detecting and Quantifying a Massive Invasion of Floating Aquatic Plants in the Río de La Plata Turbid Waters Using High Spatial Resolution Ocean Color Imagery. *Remote Sensing* **2018**, *10*, 1140, doi:10.3390/rs10071140.
10. Bintz, J.C.; Nixon, S.W. Responses of Eelgrass *Zostera marina* Seedlings to Reduced Light. *Marine Ecology Progress Series* **2001**, *223*, 133–141, doi:10.3354/MEPS223133.
11. Bertelli, C.M.; Unsworth, R.K.F. Light Stress Responses by the Eelgrass, *Zostera marina* (L). *Frontiers in Environmental Science* **2018**, *6*, 39, doi:10.3389/FENVS.2018.00039/BIBTEX.
12. Lalumière, R.; Messier, D.; Fournier, J.J.; Peter McRoy, C. Eelgrass Meadows in a Low Arctic Environment, the Northeast Coast of James Bay, Québec. *Aquatic Botany* **1994**, *47*, 303–315, doi:10.1016/0304-3770(94)90060-4.
13. COMEX. Report on the Public Consultations Held in November 2012 Following Implementation of Hydro-Quebec’s Eastmain-1-A and Sarcelle Powerhouses and Rupert Diversion Project. **2013**.
14. El-Sabh, M.I.; Koutitonsky, V.G. An Oceanographic Study of James Bay before the Completion of the La Grande Hydroelectric Complex. *ARCTIC* **1977**, *30*, 169–186, doi:10.14430/arctic2697.

15. Hydro-Quebec and GENIVAR Groupe Conseil Inc. *Environmental Monitoring of the La Grande Complex. Abridged Summary Report 1988-2000. Eelgrass Meadows of the Northeast Coast of James Bay.*; **2005**. 238p.
16. Stantec Consulting Ltd. Desktop Investigation of Eelgrass Along the Eastern Coast of James Bay. **2017**. 28p.
17. Gallant, E.; LaRocque, A.; Leblon, B.; Douglas, A. Eelgrass Mapping with Sentinel-2 and UAV Multispectral Imagery in Atlantic Canada. **2021**, 7939–7942, doi:10.1109/IGARSS47720.2021.9554760.
18. Forsey, D.; LaRocque, A.; Leblon, B.; Skinner, M.; Douglas, A. Refinements in Eelgrass Mapping at Tabusintac Bay (New Brunswick, Canada): A Comparison between Random Forest and the Maximum Likelihood Classifier. *Canadian Journal of Remote Sensing* **2020**, 46, 640–659.
19. Lalumière, R.; Lemieux, C.; Belzile, L. *Répartition De La Zostere Maiune (Zostera marina L.) Sur La Côte Nord-Est De La Baie James - Été 1996*; **1996**; 44p.
20. Wu, J.L.; Ho, C.R.; Huang, C.C.; Srivastav, A.L.; Tzeng, J.H.; Lin, Y.T. Hyperspectral Sensing for Turbid Water Quality Monitoring in Freshwater Rivers: Empirical Relationship between Reflectance and Turbidity and Total Solids. *Sensors (Switzerland)* **2014**, 14, 22670–22688, doi:10.3390/s141222670.

## Appendix

```
## Example Settings File

inputfile=C:\User\Path_To_Input_Image
output=C:\User\Path_To_Output_Folder
limit=51, -79.8, 54.8, -78.3
aerosol_correction=dark_spectrum
merge_tiles=True
dsf_path_reflectance=tiled
glint_correction=True
## L2w Parameters
l2w_parameters=rhot_*,rhos_*,rhow_*,Rrs_*,t_nechad
## Glint Correction
glint_write_rhog_ref=True
glint_write_rhog_all=True
## Masking
l2w_mask=True
l2w_mask_wave=1600
l2w_mask_water_parameters=True
l2w_mask_negative_rhow=True
l2w_mask_cirrus=True
## Output Options
rgb_rhot=False
rhb_rhos=False
l2r_export_geotiff=True
l2w_export_geotiff=True
export_geotiff_coordinates=True
xy_output=True
```

Figure A1. Text used as a settings file to direct the Acolite atmospheric correction software. Inputs can be found in the Acolite manual at <https://odnature.naturalsciences.be/remsem/software-and-data/acolite>.

## Curriculum Vitae

**Candidate's Full Name:** Kevin Robert Clyne

### Universities Attended:

- University of Maine (Orono, ME)
  - o (Bachelor of Science: Marine Science)
  - o Attended: Fall 2018 – Spring 2022
- University of New Brunswick (Fredericton, NB)
  - o (Master of Science: Environmental Management. Pursuing.)
  - o Attended: Summer 2019 – Summer 2022

### Publications:

- Clyne, K., Leblon, B., LaRocque, A., Costa, M., Leblanc, M., Rabbitskin, E., & Dunn, M. (2021). Use of Landsat-8 Oli Imagery and Local Indigenous Knowledge for Eelgrass Mapping in Eeyou Istchee. *ISPRS Annals of the Photogrammetry, Remote Sensing and Spatial Information Sciences*, V-3–2021, 15–22. <https://doi.org/10.5194/isprs-annals-v-3-2021-15-2021>

### Conference Presentations:

- Clyne, K., LaRocque, A., Leblon, B., Costa, M., Leblanc, M.L., Rabbitskin, E., Dunn, M., Eelgrass, Water turbidity and forest fire as seen from Landsat and UAV images: a case study in Eeyou Istchee. Poster presentation at the 41<sup>st</sup> Canadian Symposium on Remote Sensing: Landscapes of Change; Remote Sensing for a Sustainable Future. Virtual Event. July 13-16, 2020.
- Clyne, K., Leblon, B., LaRocque, A., Costa, M., Eelgrass Bed Mapping with Landsat-8 OLI and Traditional Ecological Knowledge in Eeyou Istchee. Oral Presentation at ArcticNet: Arctic Change 2020. Virtual Event. December 7-10, 2020.
- Clyne, K., Leblon, B., LaRocque, A., Costa, M., Leblanc, M.L., Rabbitskin, E., Dunn, M., Use of Landsat-8 and Sentinel-2 Imagery and Local Indigenous Knowledge for Mapping Eelgrass in Eeyou Istchee. Poster

presentation at Atlantic Canada Coastal Estuarine Science Society (ACCESS) Conference. Virtual Event. May 13-14, 2021.

**Awards:**

- Best Graduate Poster at Atlantic Canada Coastal Estuarine Science Society (ACCESS) Conference. May 13-14, 2021.